

ESCUELA TÉCNICA SUPERIOR DE INGENIEROS
INDUSTRIALES Y DE TELECOMUNICACIÓN

UNIVERSIDAD DE CANTABRIA



Trabajo Fin de Grado

**Validación experimental de membranas
tubulares compuestas de TiO_2 /zeolita para
la filtración y oxidación fotocatalítica de
contaminantes orgánicos en agua**
Experimental validation of TiO_2 /zeolite tubular
composite membranes for filtration and
photocatalytic oxidation of organic pollutants
in water

Para acceder al Título de
Graduada en Ingeniería Química

Autor: Aranza Denisse Vital Grappin

ACKNOWLEDGEMENTS

I would like to thank Universidad de Cantabria for allowing me to work in my bachelor thesis in this institution, as well as my university of origin Universidad Autónoma de Nuevo León, for giving me the opportunity to perform this project abroad.

I would also like to thank my thesis directors Dr. Maria José Rivero Martínez and Dr. Nazely Diban-Ibrahim Gomez for guiding me through this journey and accepting me as part of their research group; without your help this would not have been possible. Thanks a lot, Carmen Barquin, for all your help with my experiments and in the writing of this work.

Special thanks to Dr. Erika Iveth Cedillo González for giving me the opportunity of working with her at the start of my bachelor's degree and helping me find my passion. Thanks to my family, especially my mother, for always being a support and all those dishes she cooked for cheering me up, my father for those late-night coffees that he offered while working, my sister, for always listening and helping me and my brother for always getting worried for me.

I want to thank to all those people that accompanied in my journey and made me who I am today, especially my friends and colleagues. Thanks, Adrian, for always being there for me, trying to understand me and always making me laugh, thanks Emmanuel for being my greatest support in the university and my confidant. Special thanks to all those people that I met here in Santander, and sharing with me the moments that I perceive as my happiest ones. Thanks Karla, for always listening to me, understanding me and cheering me, thank you, Kaan, for those hugs that I didn't know that I missed from home, thanks Arthur, for sharing with me all those places that we went, and taking care of me, and thanks Paula, for always sharing your feelings; but mostly, thank you for being my family and my home here in Santander. Thank you very much Santander, for everything.

TABLE OF CONTENTS

LIST OF FIGURES	II
LIST OF TABLES	III
SUMMARY	IV
RESUMEN	VI
1. INTRODUCTION	1
1.1. Water availability	1
1.1.1. Remediation Technologies	6
1.2. Photocatalytic membranes	9
1.3. Background.....	12
2. OBJECTIVES	16
3. METHODOLOGY.....	17
3.1. Materials	17
3.2. Analytical method for pollutant monitoring.....	18
3.3. Experimental methodology.....	19
3.3.1. Permeability tests	19
3.3.2. Model compound filtration.....	22
3.3.3. Adsorption evaluation	24
3.3.4. Photocatalytic evaluation	25
3.3.5. Coupled photocatalysis and filtration evaluation.....	27
4. RESULTS AND DISCUSSION	29
4.1. Permeability tests.....	29
4.1.1. Model compound filtration	32
4.2. Adsorption evaluation.....	36
4.3. Photocatalytic evaluation.....	37
4.4. Coupled photocatalysis and filtration evaluation.....	39
5. CONCLUSIONS	43
6. NOMENCLATURE	44
7. BIBLIOGRAPHY	45
8. APPENDIX.....	56

LIST OF FIGURES

Figure 1. Photocatalytic mechanism.	8
Figure 2. Composition of membrane materials.	17
Figure 3. Permeability trials system. a) membrane, b) solution container, c) balance, d) vacuum trap, e) vacuum pump.	19
Figure 4. TiO ₂ membrane with fittings.	20
Figure 5. Scheme of the filtration evaluation assay.	23
Figure 6. Scheme of the non-automated fouling evaluation	23
Figure 7. Scheme of the automated fouling evaluation assays	24
Figure 8. Schematic of the membrane position in the reactor.	25
Figure 9. Schematic of photocatalytic assay's system. a) sample collection, b) magnetic stirring plate, c) cylindrical photocatalytic reactor of 1 L of capacity, d) control board	26
Figure 10. Photocatalysis paired with filtration system. a) sample collection, b) magnetic stirring plate, c) cylindrical photocatalytic reactor of 1 L of capacity, d) control board, e) vacuum trap, f) vacuum pump.	27
Figure 11. Scheme of the photocatalysis and filtration paired assays.	28
Figure 12. Water flow behavior with increase of ΔP in zeolite membranes.	30
Figure 13. TiO ₂ membrane water flow behavior with increase of ΔP	30
Figure 14. TiO ₂ -Ag membrane water flow behavior with increase of ΔP	31
Figure 15. Permeate flux change in 5 filtration cycles; each cycle duration: a) 7 min. TiO ₂ membrane, b) 11 min. TiO ₂ -Ag membrane. Flux calculated with permeate mass through time. First 5 cycles with water were performed, followed by DBS cycles and so on (washing in between).	34
Figure 16. Comparison of permeation flux; interspersed with water and DBS trials. W: Water. (Flux calculated with final volume and time). a) TiO ₂ membrane, b) TiO ₂ -Ag membrane.	35
Figure 17. DBS change in concentration through 5 filtration cycles a) each cycle duration: 9 min.; TiO ₂ membrane. b) each cycle duration: 17 min.; TiO ₂ -Ag membrane. (Flux calculated with final volume and time).	36
Figure 18. Adsorption of DBS and DCA with TiO ₂ and TiO ₂ -Ag membranes.	37
Figure 19. Experimental photocatalytic degradation and simulation of DBS and DCA with TiO ₂ and TiO ₂ -Ag membranes. Simulated data with zero-order kinetic model.	38
Figure 20. Experimental photocatalytic degradation and simulation of DBS at an initial concentration of 20 mg/L and 50 mg/L with TiO ₂ -Ag membrane.	38
Figure 21. Photocatalysis paired with filtration of DCA with TiO ₂ and TiO ₂ -Ag membranes. Photo: Concentration of DCA at reactor tank, Filt: Concentration of DCA at permeate.	40
Figure 22. Comparison of change in concentration of photocatalysis trial and photocatalysis paired with filtration trial of DCA with TiO ₂ membrane. Photo/Filt reactor C: change in concentration of DCA at reactor tank, Photo/Filt permeate C: change in concentration of DCA at permeate.	41

Figure 23. Comparison of change in concentration of photocatalysis trial and photocatalysis paired with filtration trial of DCA with TiO₂-Ag membrane. Photo/Filt reactor C: change in concentration of DCA at reactor tank, Photo/Filt permeate C: change in concentration of DCA at permeate..... 41

LIST OF TABLES

Table 1. State of the art of composite membranes.	13
Table 2. Active layer material of tested membranes	17
Table 3. Physical and chemical properties of DBS and DCA (Dichloroacetic acid CHCl ₂ COOH - PubChem no date), (Registration Dossier - ECHA no date).....	18
Table 4. Range of ΔP that were used in the permeability trials	21
Table 5. Experimental conditions set during the different fouling evaluation and DBS rejection tests.	24
Table 6. Conditions of DBS adsorption assays.	25
Table 7. Conditions of photocatalysis assays of model pollutants.	27
Table 8. Permeability summary.....	32
Table 9. Kinetic constant of different trials and its correspondent coefficient of determination.....	39

SUMMARY

Keywords

Photocatalysis, membrane filtration, photocatalytic membranes, TiO₂, TiO₂-Ag, faujasite zeolite membrane.

Scope

In recent years, along with population growth, an increase in water usage and in the generation of wastewater have been observed (UNICEF, 2019). Likewise, in water bodies, pollutants such as dichloroacetic acid (DCA) have been detected, which have been proven to be harmful (WHO, 2005); as well as emerging pollutants (Geissen, 2015), which cause different environmental impacts, but are not regulated by legislation, such as sodium dodecylbenzene sulfonate (DBS) (Li, 2020; UNEP, 2022). For the reasons described above, it is necessary to study different technologies to address this problem.

Therefore, in this work, filtration and photocatalysis tests were carried out with FAU-Na/TiO₂ and FAU-Na/ TiO₂-Ag tubular ceramic membranes for the removal of DBS and DCA; as well as the permeability analysis of faujasite zeolite membranes.

Results

Regarding the results, of FAU 03 membrane a hydraulic permeability of 10.39 L/m²h bar was obtained, for FAU 06 24.74 L/m²h bar; while for TiO₂ and TiO₂-Ag membranes hydraulic permeabilities of 745.71 and 683.87 L/m²h bar were obtained, respectively.

In the TiO₂ and TiO₂-Ag membrane filtration tests, the highest percentage of rejection obtained was 2% in both membranes. In the photocatalysis tests, the TiO₂ membrane had a degradation percentage of 16.6% of DBS and 37% of DCA, while the TiO₂-Ag membrane had a degradation percentage of 21% of DBS and 44% of DCA. In coupled photocatalysis and filtration trials, TiO₂ had an overall 59% decrease in DCA concentration, while TiO₂-Ag 67%.

Conclusions

Zeolite membranes present a hydraulic permeability similar to that reported with other authors; while photocatalytic membranes present much higher hydraulic permeabilities. The photocatalysis data in the photocatalysis alone tests were fitted to a 0-order kinetic model, while those in the photocatalysis and coupled filtration tests were fitted to a 1-order kinetic model.

The increase in contaminant degradation with TiO₂-Ag membranes is attributed to the decrease in electron and hole recombination. There is a considerable increase in the decrease in DCA concentration when pairing filtration and photocatalysis due to the increase in reactive oxygen species interaction.

References

Geissen, V., Mol, H., Klumpp, E., Umlauf, G., Nadal, M., Van Der Ploeg, M., Van De Zee, S.E.A.T.M., Ritsema, C.J., 2015. Emerging pollutants in the environment: A challenge for water resource management. *International Soil and Water Conservation Research*. Vol. 3, no. 1, pp. 57. DOI 10.1016/j.iswcr.2015.03.002.

Li, H., Yang, Y., Gao, J., Li, X., Zhou, Z., Wang, N., Du, P., Zhang, T., Feng, J., 2020. Degradation of sodium dodecyl benzenesulfonate by vacuum ultraviolet irradiation. *Journal of Water Process Engineering*. Vol. 34, pp. 101172. DOI 10.1016/j.jwpe.2020.101172.

UNEP - UN ENVIRONMENT PROGRAMME, 2022. Emerging Pollutants in Wastewater: An Increasing Threat. <http://www.unep.org/events/un-environment-event/emerging-pollutants-wastewater-increasing-threat>. 3 May 2022.

UNICEF, 2019. 1 in 3 people globally do not have access to safe drinking water. <https://www.who.int/news/item/18-06-2019-1-in-3-people-globally-do-not-have-access-to-safe-drinking-water-unicef>. 3 May 2022.

WHO, 2005. Dichloroacetic Acid in Drinking-water Background document for development of WHO Guidelines for Drinking-water Quality. https://cdn.who.int/media/docs/default-source/wash-documents/wash-chemicals/dichloroaceticacid0505.pdf?sfvrsn=2246389b_4. 13 March 2022.

RESUMEN

Palabras clave

Fotocatálisis, filtración de membrana, Membranas fotocatalíticas, TiO_2 , $\text{TiO}_2\text{-Ag}$, membrana de zeolita faujasita.

Planteamiento del problema

En los últimos años, junto con el crecimiento de la población, se ha observado un incremento en el uso del agua y en la generación de aguas residuales (UNICEF, 2019). Así mismo, en medio acuosos, se han detectado contaminantes como el ácido dicloroacético (DCA), que se ha comprobado que son dañinos (WHO, 2005); así como contaminantes emergentes (Geissen, 2015), los cuales causan diferentes impactos ambientales, pero que no se encuentran regularizados por la legislación, como el dodecibenceno sulfonato de sodio (DBS) (Li, 2020; UNEP, 2022). Por lo anterior descrito es necesario el estudio de diversas tecnologías para abordar esta problemática.

Por ello, en este trabajo se realizaron ensayos de filtración y fotocátalisis con membranas cerámicas tubulares FAU-Na/ TiO_2 y FAU-Na/ $\text{TiO}_2\text{-Ag}$ para la eliminación de DBS y DCA; así como el análisis de permeabilidad de membranas de zeolita faujasita.

Resultados

Respecto a los resultados, para la membrana FAU 03 se obtuvo una permeabilidad hidráulica de 10.39 $\text{L/m}^2\text{h bar}$, para FAU 06 24.74 $\text{L/m}^2\text{h bar}$; mientras que para las membranas de TiO_2 y $\text{TiO}_2\text{-Ag}$ se obtuvieron permeabilidades hidráulicas de 745.71 y 683.87 $\text{L/m}^2\text{h bar}$, respectivamente.

En los ensayos de filtración de la membrana de TiO_2 y de $\text{TiO}_2\text{-Ag}$, el mayor porcentaje de rechazo obtenido fue del 2%. En los ensayos de fotocátalisis, la membrana de TiO_2 tuvo un porcentaje de degradación del 16.6% del DBS y del 37% del DCA, mientras que la de $\text{TiO}_2\text{-Ag}$ del 21% del DBS y del 44% del DCA. En la fotocátalisis y la filtración acopladas, el TiO_2 tuvo una disminución total del 59% en la concentración de DCA, mientras que el $\text{TiO}_2\text{-Ag}$ del 67%.

Conclusiones

Las membranas de zeolita presentan una permeabilidad hidráulica similar a la reportada con otros autores; mientras que las membranas fotocatalíticas presentan permeabilidades hidráulicas mucho mayores. Los datos de fotocátalisis en los ensayos de fotocátalisis sola se ajustaron a un modelo de cinética de orden 0, mientras que los de fotocátalisis y filtración acoplada, a un modelo de cinética de orden 1.

El incremento en la degradación de contaminante con las membranas de TiO₂-Ag se le atribuye a la disminución de recombinación de electrones y huecos. Hay un incremento considerable de la disminución de la concentración de DCA al emparejar la filtración y la fotocátalisis debido al incremento en la interacción de especies reactivas de oxígeno.

Bibliografía

Geissen, V., Mol, H., Klumpp, E., Umlauf, G., Nadal, M., Van Der Ploeg, M., Van De Zee, S.E.A.T.M., Ritsema, C.J., 2015. Emerging pollutants in the environment: A challenge for water resource management. *International Soil and Water Conservation Research*. Vol. 3, no. 1, pp. 57. DOI 10.1016/j.iswcr.2015.03.002.

Li, H., Yang, Y., Gao, J., Li, X., Zhou, Z., Wang, N., Du, P., Zhang, T., Feng, J., 2020. Degradation of sodium dodecyl benzenesulfonate by vacuum ultraviolet irradiation. *Journal of Water Process Engineering*. Vol. 34, pp. 101172. DOI 10.1016/j.jwpe.2020.101172.

UNEP - UN ENVIRONMENT PROGRAMME, 2022. Emerging Pollutants in Wastewater: An Increasing Threat. <http://www.unep.org/events/un-environment-event/emerging-pollutants-wastewater-increasing-threat>. 3 May 2022.

UNICEF, 2019. 1 in 3 people globally do not have access to safe drinking water. <https://www.who.int/news/item/18-06-2019-1-in-3-people-globally-do-not-have-access-to-safe-drinking-water-unicef>. 3 May 2022.

WHO, 2005. Dichloroacetic Acid in Drinking-water Background document for development of WHO Guidelines for Drinking-water Quality. https://cdn.who.int/media/docs/default-source/wash-documents/wash-chemicals/dichloroaceticacid0505.pdf?sfvrsn=2246389b_4. 13 March 2022.

1. INTRODUCTION

1.1. Water availability

UNICEF (2019) reports that 2.2 billion people around the world do not have easy access to water, or access only to polluted water, therefore 1 in 3 people in the world do not have access to safe drinking water; 4.2 billion lack hygienic toilets where the wastes can be disposed of safely. As the population increases, the use of water for food production, sanitation and industrial uses has been increasing, in 2000, 3.79 trillion m³ of freshwater were extracted, which by 2014 increased to 3.99 trillion m³ (Ritchie and Roser, 2017). Worldwide, in 2018, 71.9% of the water withdrawn was used by the agriculture sector for activities such as irrigation or those related to livestock and aquaculture, 16.1% for the industrial sector and 1.2% was used for municipal direct use by the population (Tiseo, 2022). The National Institute of Statistics (INE) reports that in Spain in 2018, households consumed 2,271 hm³ of water, 1.2% less than in 2016, while in the economic sector 629 hm³ were consumed 0.6% less than in 2016; regarding municipal and other water consumption, a consumption of 288 hm³ was reported, 63% more compared to 2016; so, the average water consumption in 2018 was 133 liters per inhabitant per day (Instituto Nacional de Estadística, 2018).

In Spain in 2014 with a consumption of 32.9 billion m³ of water, 80.4% was extracted from surface water, 19.2% from groundwater and 0.5% from desalination; from 2012 to 2014, groundwater extraction decreased by 4.3%, surface water by 6.7% and obtaining water by desalination increased by 24.7% (PWC, 2018). The European Environment Agency (EEA) reports each year the water exploitation index (WEI+), of the European Union countries, which indicates the total water use as a percentage of renewable freshwater resources (groundwater and surface water), as a whole, the European union countries in 2016 (27 countries) had a WEI+ of 6.8%, which increased to 8.4% for 2017. However, specifically Spain in 2016 had a WEI+ value of 17.3%, which increased to 23.7% in 2017; it is worth noting that when you have an index greater than 20% it is considered an indicator of water scarcity (Eurostat, 2022a).

Worldwide, it is estimated that 360 km³/year of domestic and municipal wastewater are generated, of which 11.4% is treated in water treatment plants (WWTP) and reused, while 41.4% is treated and discharged and 47.2% is not treated and discharged directly to the environment, likewise, in the Middle East, North Africa and Western Europe the amount of water that is treated and reused is considerable, Middle East and Africa with a percentage of 15% of water that is treated and reused and Eastern Europe 16% (Ehalt Macedo et al., 2022). Jones et al. (2021) reports that of the total wastewater generated, 41% comes from 16% of the population living in high-income countries. In 2014 in Spain, a gain of 2.5 billion euros was achieved by purification and sanitation activities; with respect to volume, it has gone from sanitizing 2.8 million m³ in 2000, to 4.9 million m³ in 2014 (Instituto Nacional de Estadística, 2018; PWC, 2018). Likewise in 2012, 95.6% of the population in Spain had access to sewerage system, while 0.50% of the population had access to facilities with primary water treatment, 27.6% secondary treatment and 61.1% to tertiary treatment; in 2018 access to sewerage increased to 96.5%, 1.7% of the population with access to primary treatment facilities, 29.4% to secondary and 57.2% to tertiary (Eurostat, 2022b).

In the European Union there are different council directives that address the water parameters depending the water purpose or even for pollutant type; the urban wastewater treatment directive (Directive 91/271/EEC) aims to protect the environment from the effects of industrial and urban wastewater discharges, in this directive, treated effluent water parameters limits are established, such as, Biochemical oxygen demand (BOD₅), Chemical oxygen demand (COD), total suspended solids, total phosphorus, total nitrogen with values of 25 mg/L O₂, 125 mg/L O₂, 35 mg/L, 2 mg/L P and 15 mg/L N, respectively.

As well, the environmental quality standards directive (Directive 2000/60/CE) enacts the concentration limit of 33 priority substances presenting a significant risk to the aquatic environment and most of the substances presented in the list are organic substances; moreover, a bathing water directive (Directive 2006/7/EC) is also presented in which microbiological percentile values are shown, such as *Intestinal enterococci* and *Escherichia coli* (Kurrer, 2021). In Spain, 84% of the wastewater generated is treated

according to the regulations imposed by the European Union (EU) legislation, since it has 1036 plants with biological treatment with nitrogen and/or phosphorus removal, 730 with biological treatment and 33 with primary treatment (UNICEF 2019).

In Mexico, in 2020 national coverage in drinking water reached 96.1% and 95.2% for sewer system; in urban areas, in that same year, it was reported that 98.5% of sewer system's availability was reached whilst in rural areas only an 83.2%. In 2020, 348,480 liters per second of water produced and supplied to the population nationwide, a 339,290 liters per second were disinfected. In that same year, there were 2,786 plants in operation for municipal wastewater treatment, with an installed capacity of 196.7 m³/s and a treated flow of 144.7 m³/s; thus, a treatment coverage of 67.2% of collected wastewater; activated sludge is the treatment with the highest treated flow, with 75.2 m³/s, traduced as 52% of the flow treated at the national level. Regarding industrial wastewater treatment, Mexico has 3,397 industrial wastewater treatment plants; of these, 3,375 are in operation and generate a treatment flow of 71,638 liters; the most used level of treatment, at the national level, is secondary treatment, which is applied in 1,829 plants, followed by primary treatment, applied in 994 plants, and finally tertiary treatment in 99 plants (Comisión Nacional del Agua, 2021)

There are pollutants, called emerging pollutants (EPs), that can enter the environment and cause adverse effects in humans and marine life but are not regulated; thus, there are no limits established in the legislation of their emission discharge (Geissen et al., 2015). These pollutants are mainly organic compounds, such as, hormones, food additives, personal hygiene products, plasticizers, wood preservatives, pesticides, disinfectants, antibiotics, drugs, steroids, microplastics, microbeads, laundry detergents, surfactants and other compounds generated mostly by human activities (UNEP - UN Environment Programme, 2022; Tang et al., 2019); 700 substances, divided in 20 categories have been found (Geissen et al., 2015).

As well, another compound of concern is DCA, this is an organochlorine chemical made up of acetic acid with two chloro substituents at the 2-position (Dichloroacetic acid | CHCl₂COOH – PubChem, 2022). This substance, which is registered under the REACH

Regulation, is produced in or imported into the European Economic Area at a rate of between 100 and 1000 t/year (Substance Information – ECHA, 2022). Because they block the activity of the enzyme pyruvate dehydrogenase kinase, DCA salts are used as medications (Dichloroacetic acid: Uses, Interactions, Mechanism of Action | DrugBank, 2022), also as a potential oral hypoglycemic drug, thus it can be used as treatment of diabetes (Satheesh Ananda and Mehendale, 2005).

DCA has been found in rainwater, drinking-water, groundwater and surface water distribution systems and even swimming pools (WHO, 2005); is one of the most common disinfection byproducts that can be found (Kissling et al., 2009). Nonetheless, in mice, rats, dogs, and people under DCA treatment, liver damage has been demonstrated by increases in serum levels of liver enzymes. Mice treated to large doses of DCA frequently developed hepatic necrosis; also, male rats and mice exposed to DCA develop hepatic adenomas and adenocarcinomas at higher incidence and in greater numbers (EPA. After being added to drinking water, DCA enhanced the incidence of cutaneous papilloma in both males and females of the same strain as well as the bronchioloalveolar adenoma in female Tg.AC hemizygous mice (IARC, 2014).

Surfactants are substances that when added to a compound, its surface tension is reduced, thus increasing wetting and spreading properties (Britannica, 2022), this by generating micelles (self-assembled molecular clusters) and getting absorbed in the liquid-gas interface, as well in the liquid-liquid interface like oil and water (Assadi et al., 2012; Nakama, 2017). Surfactants are used as cleansers, emulsifiers, antifogging agents, deinking agents, defoaming agents and solubilizing agents, but are mostly used as detergents. The surfactants have an amphiphilic structure, inferring that its molecules consist in a hydrophilic group, meaning aversion to water, thus, soluble in lipids and hydrophobic groups, meaning that have affinity to water, therefore, soluble in water (Nakama, 2017).

Surfactants are classified into ionic and non-ionic surfactants. Additionally, ionic surfactants are classified into anionic, cationic and amphoteric surfactants; anionic are the oldest and most common type of surfactant (Ivanković and Hrenović, 2010); this can

be used as detergents, household cleaning, pesticide formulations or pharmaceutical formulations (Ivanković and Hrenović, 2010; Sumpter, 2000). Anionic surfactants are characterized by a negatively charged hydrophilic polar group that dissociated into anions in aqueous solutions (Ivanković and Hrenović, 2010; Nakama, 2017). The anionic surfactants, including alkylbenzene sulfonates, are the major constituents of synthetic detergent (Garcia et al., 2008). Among them, DBS, that is also a linear alkylbenzene sulfonate (LAS) with a chain length of C12 with the benzene connected to the C6, is one of the most employed anionic surfactants (Mungray and Kumar, 2009; Yu et al., 2006), and it is used in different chemical, biochemical and industrial applications (Dubey and Pal, 2012), in food processing, cosmetics and papermaking industries, (Gu et al., 2021) and in detergents, cleaning products and pesticides (Liu et al., 2010).

The surfactants concentration in wastewaters varies. Those at the highest concentrations are the anionic surfactants, followed by cationic ones, nevertheless, these last ones were usually found in conjunction with other anionic surfactants (Venhuis and Mehrvar, 2004). Clara et al. (2007) analyzed nine municipal WWTPs in western Australia where they found a LAS influent concentration that varied from 2.4 to 6.7 mg/L whilst effluent concentrations were about 11 to 50 µg/L (Palmer and Hatley, 2018). Zhu et al. (2018) studied in Harbin, China, the influent and effluent of different surfactants in two typical industrial and domestic WWTPs. They found that the LAS C12 was one of the most predominant surfactants in the influent with a concentration that varied between 8.02 - 674 µg/L, also that the concentration of effluent was substantially lower than that of influent, showing that the two WWTPs were very effective at removing these contaminants. Regardless of the efficiency of LAS removal that some authors report, it has been found that LAS at concentrations akin in WWTPs outlets increases the growth rate of intestinal cancer cells (Bradai et al., 2016). Even though a large number of studies have shown that most commercial surfactants can be degraded in an aerobic medium at low concentrations, this biodegradability may be hampered in anaerobic media or when the surfactants are present at high concentrations, as in the effluent from industrial processes and other technologies using surfactants for recovery (Bautista-Toledo et al., 2014). Although initial microbial degradation of LAS by the residential and industrial activated sludge microbial population is efficient, most of the

associated metabolites cannot be mineralized (Bautista-Toledo et al., 2014; Nielsen et al. 1997).

1.1.1. Remediation Technologies

Surfactants cause many difficulties in WWTP. Therefore, phytoremediation, ultrasonic irradiation, microwave irradiation, vacuum ultraviolet irradiation, ozonation, electrochemical oxidation, bioadsorption/biodegradation, coagulation and flocculation, zerovalent iron, membrane filtration or photocatalysis (Bhandari and Gogate, 2019; Li et al., 2020; Manousaki et al., 2004; Masoudian et al., 2020; Zhang et al., 2009) have been tested for their removal. *Azolla filiculoides* was used for studying DBS biodegradation, they proved that degradation was possible at certain conditions, nonetheless, *Azolla* plant tends to grow in temperate to tropical zones, therefore it may not be able to withstand all weather conditions (Masoudian et al., 2020). There are also treatments that are used as a support for the main degradation system, such as ultrasonic irradiation and microwave irradiation (Bhandari and Gogate, 2019; Manousaki et al., 2004; Zhang et al., 2009). Similarly, there are treatments as vacuum ultraviolet irradiation that has reported a degradation of 66.4% for 180 min irradiation (Li et al., 2020), there are also reports on ozonation that mention that this treatment can partially remove surfactant and Chemical Oxygen Demand (COD) from municipal wastewater even under ideal working conditions; but does change the molecular structures of the organic matter into simpler ones, therefore it is recommended pairing this treatment with another biological one (Beltrán et al., 2000), coagulation and flocculation has also been reported as an effective way to remove DBS from water systems, even so, this treatment just immobilizes the pollutant yet does not degrade it (Beltrán-Heredia et al., 2009). Adsorption has been another studied treatment. Taffarel et al. (2010) investigated the adsorption of DBS on natural Chilean zeolite with cetyl trimethylammonium bromide and achieved a maximum adsorption capacity of 30.7 mg/g (Taffarel and Rubio, 2010).

Membrane filtration is an advanced separation technology where microporous barriers made of polymeric, ceramic, or metallic materials are used to separate dissolved

substances (solutes), colloids, or small particulates from solutions (Eccles, 1997). Membranes can be classified based on the mean membrane pore size and pore type (Pendergast and Hoek, 2011):

- Microfiltration (MF): ranges a pore of 50-500 nm (macropores). It is used for insoluble particulate materials, as oil emulsion, yeast, fungi and bacteria.
- Ultrafiltration (UF): it ranges a pore size of 2-50 nm (mesopores) and can separate colloidal solids, humics/nucleic acids, proteins/polysaccharides and viruses.
- Nanofiltration (NF): pore sizes ≤ 2 nm (micropores); it can separate sugars, divalent salts and common antibiotics.
- Reverse Osmosis (RO): pore sizes of 0.3-0.6 nm (micropores); it can separate organic antibiotics and monovalent salts.

Membrane filtration advantages are: lower operating and maintenance costs, simple to use and provide more consistent results, and most contaminants in the wastewater stream can be reduced or eliminated in one step, also the permeate can be reused, resulting in water conservation and a reduction in raw water use (Chen et al., 2006): Moreover, it does not require chemical additives, it is modular and easy to scale-up (Buonomenna, 2016). Membranes such as ceramic ultrafiltration membranes, nanofiltration commercial membranes and ultrafiltration flat membranes, have been used for studying the filtration of DBS as an alternative of traditional treatment. These have had different retention percentages, depending on the type of membrane, transmembrane pressure, concentration, among other parameters (Boussu et al., 2007; Kim and Park, 2021; Moulai-Mostefa et al., 2007; Tu et al., 2009).

Photocatalysis is a photoinduced process that is facilitated by the presence of a catalyst, also described as a chemical reaction that occurs when light and the photocatalyst interact (Madjene et al., 2013; Zhang et al., 2019). These reactions are triggered by the absorption of a sufficiently energetic photon, meaning equally or higher than the band-gap energy of the catalyst. This band-gap energy can be expressed as the energy difference between the valence band and the conduction band. The absorption causes a charge separation by promoting an electron (e^-) from the semiconductor catalyst's

valence band to the conduction band, resulting in a hole (h^+) in the valence band (Ameta et al., 2018; Madjene et al., 2013). This process is shown in Figure 1. An electric field separates photogenerated electrons and holes, which then migrate to the surface of semiconductor particles. The electron–hole pairs move to the semiconductor surface individually and participate in a sequence of oxidation/reduction events with adsorbed species like water and oxygen to produce highly reactive oxygen species (ROS) (Chakhtouna et al., 2021). ROS have high oxidizing characteristics and can oxidize molecules adsorbed on the semiconductor's surface or in its solution (Zhang et al., 2019). Main advantages of this advanced oxidation process (AOP) are the lack of addition of extra chemicals, the oxidant agent is not consumed during the oxidation (Diban et al., 2021), it works at ambient pressure and temperature and it is a very attractive alternative because, mineralization of organic compound to carbon dioxide is possible (Zhang et al., 2019).

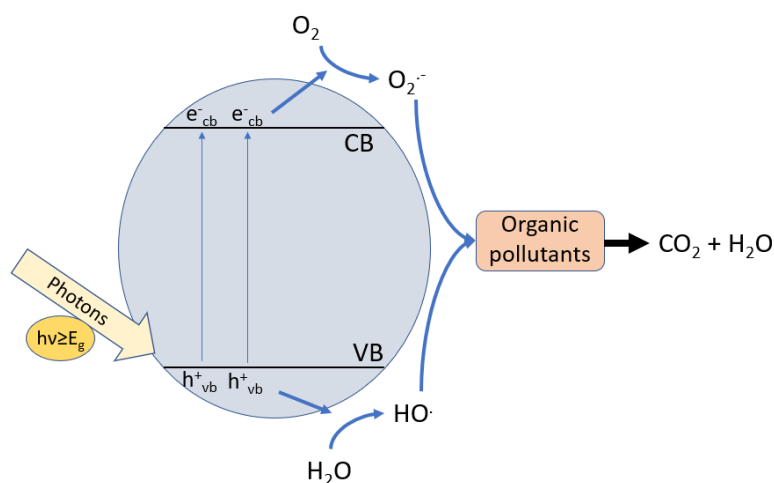


Figure 1. Photocatalytic mechanism.

Even though there are many advantages with membrane filtration and photocatalysis, both have some issues. In the case of membranes, fouling is the blocking of the membranes pores due to mechanical action or physical and chemical interactions of the solute macromolecules onto the membrane (Liu et al., 2019). In photocatalysis one of the main hindrances is the suspended photocatalyst that makes the handling of the system difficult, as well as the long degradation times for the pollutants (Geissen et al., 2001). Because of the drawbacks that photocatalysis and membrane filtration pose, an

approach was made by merging these two treatments, thus immobilizing the photocatalyst, reducing pollutant removal time and avoiding membrane blocking.

1.2. Photocatalytic membranes

There are many types of membranes depending on their material, and they can be divided into two main categories, inorganic, and polymeric membranes. There are also thin layer composite membranes that can be either polymeric or inorganic depending the support (Pendergast and Hoek, 2011). These composite membranes have been drawing more attention, and they consist of a thin barrier polymerized over a porous polymeric support membrane or a ceramic membrane. Therefore, the membrane is made up of two (or more) layers that serve different functions in the separation: the active layer, which can be porous or dense depending on the membrane operation, this is the first layer in contact with the feed solution and is the layer that actually filtrates. Then there is the porous sublayer(s), that acts as mechanical support and it merely offers mechanical strength to the membrane allowing high-pressure activities (Buonomenna, 2016). This type of membrane has different advantages, such as independent material selection for the porous support and thin layer that allows each structural element to be optimized, and finally, expensive membrane materials can be used because only a small amount of polymer is required (Pinnau, 2000).

Ceramic membranes have much better performance than polymeric, long service life, chemical stability, hydrophilicity, temperature and morphological stability, in the temperature range of 130 to 250°C, as well as non-deformability (Kotobuki et al., 2021; Kotrotsiou and Kiparissides, 2019), just like the zeolite-coated membranes. Zeolites are hydrated aluminosilicate assembled via the interlinkage of oxygen atoms of tetrahedral alumina (AlO_4^{5-}) and silica (SiO_4^{4-}) with crystalline formations on the sub-nanometer and nanometer scales that are very homogeneous. The zeolite primary building unit structure is formed of center atoms, like Al, Si, or P, and a terminal oxygen atom in a tetrahedral structure. Thus, the center atom is the vertex that connects four oxygen atoms. It can also form secondary building units, with shapes such as prisms, rings, and other shapes (Derbe et al., 2021; Pendergast and Hoek, 2011). Zeolites have a number

of unique qualities due to their unusual structure, for instance, good shape-selectivity, that refers to the presence of channels and chambers with well-defined dimensions, capacity to exchange ions, large volume of free space and low density, adsorbent of molecules and ions and catalytic potential (Król, 2020).

The zeolites can be classified into two main groups, natural and synthetic. Natural zeolites, such as chabazite, clinoptilolite, and mordenite, these are mostly generated from volcanic and sedimentary rocks but also hydrothermal. Even with their wide applications, they have limited industrial applications since their qualities are solely determined by their crystal structure, and their channel diameters tend to be too small. Natural zeolites do not allow bigger gas molecules and organic compounds to adsorb; instead, synthetic zeolites, that are synthesized through different methods, compared to natural zeolites, have a substantially higher adsorption capacity for heavy metal ions, larger pore size, Al content can be adjusted, higher ionic exchange capacity and larger specific surface area (Derbe et al., 2021; Król, 2020). As well, synthetic zeolites can be classified into different categories, according to the framework topology, for example, zeolite A, zeolite P, zeolite N-A, zeolite H, zeolite L, zeolite O, zeolite ZK-4, zeolite ZK-5, Zeolites Ω , zeolite X and zeolite Y (Synthetic zeolites - structure, classification, current trends in zeolite synthesis review, 2022). This last two are subcategories of faujasite type framework (FAU), that is an aluminosilicate having 1.3 nm-diameter cavities joined by 0.74 nm-diameter pores, and is divided into zeolite X and zeolite Y depending their Si/Al molar ratio, X-type have a Si/Al molar ratio of 1.0–1.5 and Y-type have a Si/Al molar ratio bigger than 1.5 (Reinoso et al., 2018). Because zeolites have a wide range of industrial applications, such as adsorbent, gas separator, purificator, separation membrane, catalytic membrane reactor, chemical sensor, electrode, opto-electronic device, protection or insulation layer; supported zeolite layers have attracted intense research efforts in the last decade (Caro and Noack, 2008).

FAU zeolite membranes have been used for different purposes. Basumatary et al. (2016) used FAU zeolite, constructed on a circular shaped porous ceramic support, to remove Cr(VI) from aqueous solution in a cross flow mode; 82% of removal was achieved at a pressure of 345 kPa and a $1.11 \times 10^{-7} \text{ m}^3/\text{s}$ flow rate; these composite membranes, due

to the zeolite, have also adsorption features. Therefore, having a dual function of membrane filtration and adsorption that can help to effectively remove trace levels of contaminants such as cationic heavy metals, anionic phosphates, and nitrates (Khulbe and Matsuura, 2018). Nonetheless, there is no much research about surfactant removal with the use of zeolite membranes, but the work published by Workneh (2008) in which they used a sodalite octahydrate zeolite-clay composite membrane for the separation of sodium dodecyl sulfate (SDS). The membrane showed a rejection in the range of 10–45% having an SDS concentration greater than the critical micelle concentration (CMC).

For inducing a series of reductive and oxidative processes on its surface, the semiconductor TiO_2 has been widely used as a photocatalyst (Madjene et al., 2013). This photocatalyst has also been recognized as one with the best performances (Moura and Picão, 2022). Rutile, brookite, and anatase are the three crystal forms of TiO_2 . Anatase and rutile-type TiO_2 are the most often employed photocatalysts among these three crystal forms (Huang et al., 2015; Zhang et al., 2019). And because the band-gap of anatase TiO_2 is 3.2 eV for anatase and 3.0 eV for rutile, a photonic band-gap in the mid-to-high UV wavelength region (280–380 nm) is required for the e^- to move to the conduction band (Duan et al., 2019; Nakata and Fujishima, 2012). Unfortunately, when compared to visible light that accounts 45% of the solar spectrum, UV only accounts for 5% (Chakhtouna et al., 2021). TiO_2 photocatalysis is a well-known photocatalytic environmental cleaner, particularly for water purification (Ochiai and Fujishima, 2012), nonetheless it has disadvantages, including a wide band-gap and a high rate of photogenerated electron and hole recombination, and in its powder form makes the handling more difficult, and it diminishes as well its cost-effectiveness separation, because of the requirement of a recovery step for photocatalyst reuse (Duan et al., 2019; Ochiai and Fujishima, 2012). Therefore, come solutions proposed for these issues have been addressed with the photocatalyst immobilization, as in ceramic membranes (Zhang et al., 2006), and by doping or depositing other materials like zeolites (Diban et al., 2021) or metals, like silver (Ag) (Abbad et al., 2020).

Silver can trap excited electrons from TiO_2 and leave holes for the organic species degradation reactions; it can also reduce the band-gap energy, thus extending the

absorption to the visible range (Abbad et al., 2020; Seery et al., 2007), it also enhances the anatase to rutile transformation increasing the specific surface area (Chao et al., 2003). Diban et al. (2021) mixed TiO₂ and Ag deposited in TiO₂ with zeolites (ZY) and reported that the TiO₂-ZY composite does maintain photocatalytic activity, whilst TiO₂-Ag-ZY do not contribute to the enhancement of photocatalytic activity more than that already possessed by TiO₂. The viability of photocatalytic membranes is reaffirmed due to the handling challenges and cost-effectiveness that powdered photocatalysts face to.

Photocatalytic membranes (PMs) are those where a semiconductor-based reactive surface (e.g., titania, zinc oxide, ferric oxide) is applied to the membrane (Pendergast and Hoek, 2011). Due to its dual action over pollutants, retention/rejection/repulsion and photodegradation, PMs can provide extensive wastewater treatment, though, antifouling, lower concentration in retentate effluent, higher flux, and typically a more hydrophilic character are still issues to be considered (Pastrana-Martínez et al., 2021). PMs address two main concerns when working with membrane filtration, one of them is that the membrane filtering procedure merely concentrates contaminants to high concentrations, requiring additional treatment before discharge, and the other is the pore blockage, causing pollutant concentration in permeate. Therefore, under UV light irradiation, PMs breakdown pollutants and generate oxygen-reactive radicals, which prevents cake layer formation on the membrane surface and, as a result, reduces pore plugging hence, superior permeate quality (Riaz, 2020).

1.3. Background

The photocatalyst can be immobilized in the membrane by coating, blending into the polymeric membrane matrix, or using a free-standing membrane consisting of pure photocatalyst (Pastrana-Martínez et al., 2021). Different paths of photocatalyst synthesis and active layer deposition have been explored, such as secondary growth method (Kumakiri et al., 2014) and sol-gel synthesis method, with a dip-coating deposition technique (Zhang et al., 2006).

Table 1. State of the art of composite membranes.

Active layer material	Support material/ membrane type	Photocatalyst Synthesis method	Deposition/ embedding technique	Compound to degrade/ retain	Reference
TiO ₂ / clinoptilolite	Polyvinylidene difluoride (PVDF)/ dual layer hollow fiber (DLHF)	Solid-state dispersion	Outer dope as a mixture of PVDF and active material	Reactive Black 5	(Dzinun et al., 2019)
TiO ₂	γ -alumina UF tubular membranes	Chemical vapour deposition	Layer-by-layer deposition	Azo dye	(Athanasakou et al., 2012)
N,Pd co-doped TiO ₂	Polysulfone (PSf)	Sol-gel	Phase inversion	Eosin Yellow (EY)	(Kuvarega et al., 2018)
N-TiO ₂	γ -alumina UF tubular membrane substrates	Sol-gel	Dip-coating	methylene blue (MB); methyl orange (MO)	(Athanasakou et al., 2015)
Nanostructured TiO ₂	Alumina	Sol-gel	Spin-coated	Congo red dye	(Ahmad et al., 2017a)
TiO ₂ /ZrO ₂	α -alumina supported mesoporous γ -alumina nanofiltration membranes	Sol-gel	Dip-coating	n.a.	(Guo et al., 2018)
TiO ₂	Anodized aluminum oxide	Atomic layer deposition.		MB	(Berger et al., 2020)
TiO ₂	Home-made porous alumina substrate	Sol-gel	Dip-coating	Polyethylene glycol	(Choi et al., 2006)
TiO ₂	Home-made ceramic flat sheet membrane	Commercial P25	Dip-coating	Humic acid	(Alias et al., 2018)
Silica/titania	Alumina nanorods/nanotubes	Sol-gel	Dip-coating	DBS	(Zhang et al., 2006)
Organized mesoporous TiO ₂	Porous alumina support	Sol-gel	Spin-coated	Congo Red dye	(Ahmad et al., 2017b)

n.a. Not available

For the treatment of industrial wastewater, polymeric membranes are the most often utilized membrane. The material instability of these membranes, limits their uses. Nonetheless, ceramic membranes, particularly alumina (Al₂O₃) membranes, have been extensively explored as supports and, due to their excellent chemical and thermal durability, are the best feasible replacements to these unstable polymeric membranes (Leong et al., 2014; Pastrana-Martínez et al., 2021; Riaz and Park, 2020). Because of its

low cost, non-toxicity, and chemical stability, TiO_2 is the most often utilized material for PMs manufacturing, and usually polymer and ceramic membranes are utilized as supports for these PMs; thus, combining the titania photocatalytic layers and ceramic supports, the features of these two materials can be exploited to generate an efficient treatment system (Leong et al., 2014). Table 1 shows a summary of TiO_2 PMs.

Zhang et al. (2006) published experimental data on the elimination of DBS utilizing a photocatalytic silica/titania nanorods/nanotubes composite membrane, in which they tested the membranes with different approaches. One experiment was only testing the surfactant removal with filtration, another one the photocatalytic capacity and lastly the photocatalytic and filtration capacity altogether. The results showed that although photocatalysis did not entirely decomposed DBS, the degradation of the DBS contributed in enhancing composite membrane flow and preventing membrane fouling, that is the plugging of the pores that causes a decrease in membrane flux. Hence, these results suggest that photocatalytic membranes are a good approach for addressing membrane fouling and achieving higher removal rates of pollutants. Alias et al. (2018) worked with flat sheet porous ceramic membranes coated with TiO_2 nanoparticles and characterized them. They dip coated the membranes at different titania concentrations and also tested them with and without thermal treatment and as a result, they found that by increasing the coating concentration of TiO_2 particles the antifouling properties of the membrane increased. Zeolite and titania composites membranes have also been studied but mostly for oil-water emulsion separation (Peyravi et al., 2021), or sheets for adsorption paired with photocatalysis for pollutants removal (Fukahori et al., 2003; Xiang et al., 2017). There are many studies that report pollutant removal with zeolite membranes (Workneh, 2008), titania membranes (Zhang et al., 2006), titania coupled with metallic elements membranes (Shareef, 2020) and zeolite/titania/titania-metallic element composites (Diban et al., 2021). Nonetheless, there are no many studies in pollutant removal with zeolite/titania/titania-metallic element composite membranes; Dzinun et al. (2019) synthesized TiO_2 /clinoptilolite photocatalyst and implanted it at the outer layer of dual layer hollow fiber; this resulted in 86% of Reactive Black 5 photocatalytic degradation obtained within 60 minutes.

Therefore, the lack of investigation in surfactant removal with zeolite/TiO₂ and zeolite/TiO₂-Ag composite membranes open a new path of research. Therefore, in this work, experiments of filtration and photocatalysis with FAU-Na/TiO₂ and FAU-Na/TiO₂-Ag tubular ceramic membranes were carried out for DBS and DCA removal.

This work was carried out in the Department of Chemical and Biomolecular Engineering in the UC. The research group has previous experience on membrane technologies (Diban et al., 2008a; Diban et al., 2008b; Diban et al., 2013a; Diban et al., 2013b; Diban et al., 2021; Sánchez-González et al., 2018; Romay et al., 2020; Mantecón-Oria et al., 2020) and photocatalytic treatment (Diban et al., 2021; Dominguez et al., 2015; Ferreiro et al., 2019; Ribao et al., 2017; Ribao et al., 2018; Ribao et al., 2019; Rivero et al., 2020; Romay et al., 2020; Sanchez et al., 2011).

This work was carried out in the frame of an international project XMEM (Outperforming Functionality: Composite/Mixed Matrix Porous Materials in Membrane-based Processes), in collaboration with professor Izumi Kumakiri from University of Yamaguchi (Japan).

2. OBJECTIVES

Membranes are a technology with a high feasibility of use for the treatment of water contaminated with organic compounds. Coupling this technology with photocatalysis is a proposal for an innovative system for the mitigation of pollutants. Therefore, the objective of this work is the evaluation of the performance of novel photocatalytic tubular membranes FAU-Na/TiO₂ and FAU-Na/TiO₂-Ag for the filtration and photocatalytic degradation of dodecylbenzene sulfonate (DBS), which is a surfactant frequently used in detergents, and dichloroacetic acid (DCA) which can be also considered as an emerging pollutant as model organic contaminants in waters.

3. METHODOLOGY

3.1. Materials

The four membranes object of the present work were manufactured by the research group of Dr. Izumi Kumakiri, from Environmental Science and Engineering, Graduate School of Science and Engineering, Yamaguchi University.

The membrane's supports were porous ceramic tubes, porous α -Al₂O₃ tubes with an outer diameter of 12 mm, inner diameter of 9 mm; porosity 33%, mean pore size 1.0 μ m. The membranes have hydrophilic properties. Two of the membranes had a zeolite active layer, while the other two had a composite photocatalyst/zeolite active layer. The active layers material of the characterized membranes are shown in table 2. The samples TiO₂ and TiO₂-Ag are the photocatalytic membranes. A scheme with the membrane layers composition is shown in Figure 2. The details of the membrane synthesis method are out of the scope of this project.

Table 2. Active layer material of tested membranes

Sample name	Active layer material
FAU 03	Na-FAU
FAU 06	Na-FAU
TiO ₂	Na-FAU and TiO ₂
TiO ₂ -Ag	Na-FAU and TiO ₂ -Ag

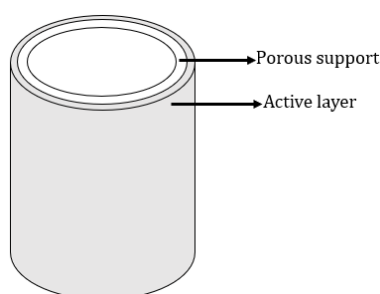
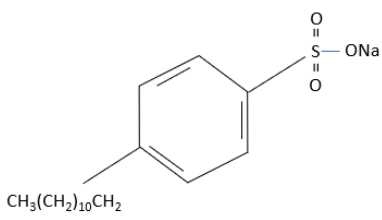
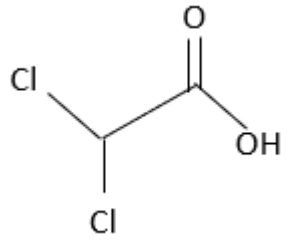


Figure 2. Composition of membrane materials.

The membrane area varied throughout the experiments, due to the fragility of the membranes that broke frequently during the connection and disconnection to the filtration system fittings. For the permeability and filtration assays, the change in membrane area does not affect the flux result, since it is taken into account for the calculations. However, for the photocatalysis and adsorption assays, the change in membrane area could affect the percentage degradation of the pollutants. Therefore, the membrane area is specified in these assays.

Model pollutants DBS and DCA were used in photocatalytic membrane filtration, adsorption and photocatalysis assays. DBS and DCA were acquired from Sigma-Aldrich Chemie GmbH (Buchs, Switzerland) and Acros Organics (ThermoFisher Scientific, Geel, Belgium) respectively.

Table 3. Physical and chemical properties of DBS and DCA (Dichloroacetic acid | CHCl_2COOH - PubChem no date), (Registration Dossier - ECHA no date).

Property/Model contaminant	DBS	DCA
Molecular formula	$\text{CH}_3(\text{CH}_2)_{11}\text{C}_6\text{H}_4\text{SO}_3\text{Na}$	CHCl_2COOH
Molecular weight (g/mol)	348.48	128.94
Water solubility (mg/L)	100 mg/L (at 25°C)	1000000 mg/L (at 20 °C)
Chemical structure		

3.2. Analytical method for pollutant monitoring

DBS was determined by UV spectrophotometry (UV-1800, Shimadzu Europe, Duisburg, Germany) at a wavelength of 223 nm. For UV spectrophotometry, a calibration curve was made by preparing DBS standard solutions with concentrations ranging from 0 to 60 mg/L. (Figure 1A). The concentration of DCA was determined using an AS9-HC column in an ICS-5000 (Dionex, ThermoFisher Scientific, Waltham, MA, USA) ion chromatograph with a 9 mM Na₂CO₃ solution as the eluent, at a flow rate of 1 mL/min and a pressure of around 2000 psi.

3.3. Experimental methodology

3.3.1. Permeability tests

Filtration properties of the membranes of water and DBS model solutions were evaluated. For the permeability assays, it was used a system consisting of a vacuum pump (Millivac Maxi SD1P014M04, Millipore) connected to a vacuum trap, which in turn was connected to the membrane and submerged under ultrapure water (MilliQ, Millipore). The vacuum trap was also placed on a balance (PS 6000.R2, RADWAG Wagi Elektroniczn). The system is presented in Figure 3. With this system, when the vacuum was pumped, the water was sucked through the pores of the membrane and caught in the vacuum trap. As well, the permeability was operated through two different systems, one of them was performed using tube plugs and teflon tape. Nonetheless, afterwards, customized fittings were manufactured through SERTO enterprise to fit in the membrane sides (Fig. 4); one of the sides was connected to the tubes that connected to the vacuum trap, while the other side was covered with a plug.

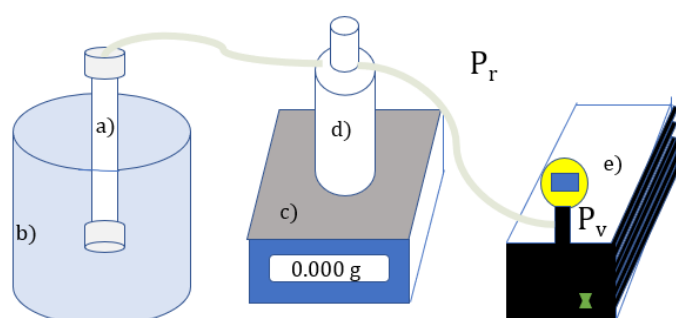


Figure 3. Permeability trials system. a) membrane, b) solution container, c) balance, d) vacuum trap, e) vacuum pump.



Figure 4. *TiO₂ membrane with fittings.*

The assays were carried out at a water temperature of 22 ± 1 °C and at different levels of vacuum pressures. The pump did not allow establishing a fixed vacuum pressure, since it was regulated through a valve; therefore, over time the pressure varied slightly due to the movement of this valve. Thus, the pressure displayed on the pump was taken every 10 minutes for the zeolite membrane samples, while for the photocatalytic membranes the pressure was recorded every minute. This was done to obtain an average pressure for each assay; the permeability trials were carried out for one hour for the zeolite membrane samples and 5 ± 2 minutes for the TiO₂ sample, while for the TiO₂-Ag sample the assays were carried out for 6 ± 2 minutes, depending on the vacuum pressure at which they were performed. In the photocatalytic membranes the vacuum trap was filled quickly, since the permeability of the water turned out to be high, this caused the permeability trials in these membranes to be much shorter than the membranes with pure zeolite, and also to a more complicated handling in terms of control of the experimental time between assays. Therefore, the average pressure obtained was used to calculate the pressure difference (ΔP) in the membrane.

Having a reference pressure (P_r) of 1070 mbar, ΔP was calculated as shown in the equation (1). Three ΔP ranges were proposed, taking into account the conditions that the system allowed; in table 4 the pressure range is presented.

$$\Delta P = P_r - P_v \quad (\text{eq. 1})$$

Where P_r is the Pressure reference and P_v is the vacuum pressure (Fig.3).

Table 4. Range of ΔP that were used in the permeability trials

Pressure level	ΔP (bar)
Low	0.944-0.974
Medium	0.997-1.022
High	1.037-1.067

The permeate flux of water through the membranes (J_w) was first computed to determine the hydraulic permeability (K_w). The water mass data (W) was registered throughout time, the data was recorded in a program (Pomiar Win) coupled with the balance; W was plotted with time at each set pressure value, thus with the slope obtained through a linear regression of the change in mass through time (eq. 2), the water density conversion and the membrane area, the different permeate fluxes were obtained (eq. 3). The value of the slope of the graph that corresponds to the hydraulic permeability of each membrane was extracted (eq. 4) by plotting the permeate fluxes obtained at each pressure setting versus ΔP and performing a linear regression. The linear regression is calculated using Microsoft Excel, that uses the least squares method. The square of the Pearson (R^2) was calculated through excel formula RSQ that uses the square of equation (5). Likewise, permeability data was also treated by equaling the predictor variables in the model to zero (when data intercepts 0).

$$W(g) = m (g \cdot h^{-1}) \cdot \Delta t(h) \quad (\text{eq. 2})$$

$$J_w(L \cdot m^2 \cdot h^{-1}) = \frac{m (g h^{-1})}{A_e (m^2) \rho (g L^{-1})} \quad (\text{eq. 3})$$

$$J_w(L \cdot m^2 \cdot h^{-1}) = K_w (L \cdot m^{-2} \cdot h^{-1} \cdot bar^{-1}) \cdot \Delta P (bar) \quad (\text{eq. 4})$$

$$r = \frac{\sum(x-\bar{x})(y-\bar{y})}{\sqrt{\sum(x-\bar{x})^2 \sum(y-\bar{y})^2}} \quad (\text{eq. 5})$$

3.3.2. Model compound filtration

For the assays of DBS filtration with the photocatalytic membranes the same system as in the hydraulic permeability assays was used (Fig. 3). The feed solution was continuously filled with a new DBS solution with a concentration of 50 mg/L, for the solution to always cover the membrane. That being the case, the membrane filtration process was carried through two different systems; both had the same system connection between the membrane and the vacuum pump, nonetheless, one was automated monitored, and the other was not; accordingly, for non-automated monitoring assays the permeate flux was calculated through equation (6); for non-automated assays the volume (V) and time (Δt) at the end of the experiment were monitored. In the automated monitored ones, change in mass was continuously monitored, thus, the permeate flux was calculated as in the hydraulic permeability tests, following equations (2-4).

$$J = \frac{V(L)}{Ae(m^2)\Delta t(h)} \quad (eq. 6)$$

For the filtration assays of DBS, the rejection percentage was calculated as shown in equation (7).

$$R(\%) = \left[1 - \frac{c_0}{c}\right] \times 100 \quad (eq. 7)$$

Three types of assays were performed for the filtration of DBS with the photocatalytic membranes. One assay, called filtration evaluation, was performed to observe the rejection of DBS over a period of 5 cycles, which was repeated 3 times with the two photocatalytic membranes. Between each cycle no washing was performed. However, between each assay, a superficial wash of the membrane was performed by pouring MilliQ water from a wash bottle for one minute. These assays were non-automated monitored. A scheme of the process is shown in Figure 5.



Figure 5. Scheme of the filtration evaluation assay.

Non-automated fouling evaluation assay consisted of performing a trial to verify the water flux prior to filtration with DBS, to later verify the filtration with DBS; hence, assays with the DBS filtration with the membrane were performed, followed by a washing and finally the water flux was tested again, to test the membrane washing efficiency (Fig. 6). These assays were not automated monitored. The system was employed with vacuum pressure, because the film of zeolite/photocatalyst was placed on the outer surface of the ceramic support membrane. Therefore, by operating the system through vacuum, if a cake layer formed on the outside of the membrane, causing fouling, the photocatalyst that is in the surface would help by degrading the pollutant on the membrane exterior in filtration/photocatalysis paired systems. Likewise, placing the photocatalyst on the exterior surface allows more easily and efficiently the light irradiation.



Figure 6. Scheme of the non-automated fouling evaluation

Finally, automated fouling evaluation assays were performed. W was measured over time for 5 cycles of 6 minutes for TiO_2 and 8 minutes for $\text{TiO}_2\text{-Ag}$, to obtain the permeate flux; then the change in mass through time was monitored during 7 min. per cycle for TiO_2 and 11 min. per cycle for $\text{TiO}_2\text{-Ag}$ with DBS, thus recording the permeate flux and the change in concentration; after the DBS assays the membrane was washed. Afterwards, 5 cycles with water were performed again and finally the DBS assays were repeated as described above (Fig. 7). Membrane model compound filtration trials conditions were as presented in table 5.



Figure 7. Scheme of the automated fouling evaluation assays

Table 5. Experimental conditions set during the different fouling evaluation and DBS rejection tests.

Sample/Assay	ΔP (mbar)	Water Temperature ($^{\circ}C$)	DBS Temperature ($^{\circ}C$)
TiO ₂ DBS cycle	0.973 \pm 0.003	n.m.	21 \pm 1
TiO ₂ -Ag DBS cycle	0.973 \pm 0.007	n.m.	21 \pm 1
TiO ₂ DBS/Water	0.966 \pm 0.003	22.7 \pm 0.2	22 \pm 0
TiO ₂ -Ag DBS/Water	0.970 \pm 0.001	23 \pm 0.9	21.8 \pm 0.6
TiO ₂ 5 DBS/5 Water	0.972 \pm 0.002	22.5 \pm 0.9	21 \pm 0.1
TiO ₂ -Ag 5 DBS/5 Water	0.967.5 \pm 0.004	23.5 \pm 0.6	22.6 \pm 1.1

n.m. Not monitored.

3.3.3. Adsorption evaluation

Organic adsorption assays in the photocatalytic membranes were carried out in a photocatalytic reactor of the APRIA SYSTEMS company, under constant stirring under dark conditions. The equipment consisted of UV-A technology that emits at a fixed wavelength of 365 nm. It consists of a dark PVC housing (height 415 mm, diameter 210 mm) with a cylindrical Pyrex glass reactor of 1 L capacity (height 250 mm, diameter 74 mm) inside; the housing has 10 strips with 3 LEDs LZ1-00UV00 (LED ENGIN). The membrane was placed in the middle of the container inside the reactor. A cover was placed so that the membrane remained in the center of the container (Figure 8).

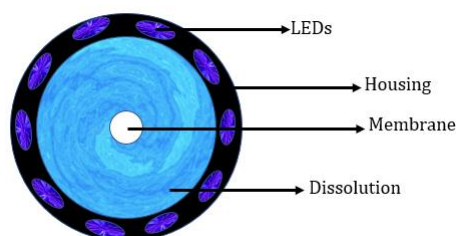


Figure 8. Schematic of the membrane position in the reactor.

The assays lasted 2 hours. DBS adsorption assays were performed with the TiO₂-Ag and TiO₂ membrane, with an initial concentration of 50 mg/L. Regarding DCA adsorption, assays were performed with the two membranes with an initial concentration of 50 mg/L. For the assays, aliquots were taken for the analysis of the change in concentration at established times. It is imperative to note that the volume of the solution should not vary by more than 20% in order for the data to be representative, i.e., the volume to be collected from the samples cannot exceed 200 mL, accordingly, the DBS aliquots had a volume of approximately 2 mL, while in the DCA assays, samples were taken at the same established times as the DBS trials, however, with aliquots of approximately 5 mL. Adsorption conditions are shown in table 6.

Table 6. Conditions of DBS adsorption assays.

Sample	Temperature (°C)	pH ₀	Membrane area (cm ²)
TiO ₂ /DBS	22.4±0.9	5.6	29.03
TiO ₂ -Ag/DBS	n.m.	n.m.	30.16
TiO ₂ /DCA	25±0.9	3.42	24.12
TiO ₂ -Ag/DCA	24.6±1.4	3.44	26.77

n.m. Not monitored

3.3.4. Photocatalytic evaluation

For the membranes photocatalysis performance of the two pollutants, DBS and DCA, were analyzed using the same APRIA SYSTEMS photocatalytic reactor used during the adsorption tests. The 10 strips with 3 LEDs LZ1-00UV00 (LED ENGINE) distributed on its inner wall in the housing of the reactor, are placed at a distance of 1.50 cm from the

solution, with an irradiance of the LEDs of 2143 W/m^2 . The reactor was placed on a stirrer to constantly stir the solution. A schematic of the system is shown in Figure 9.

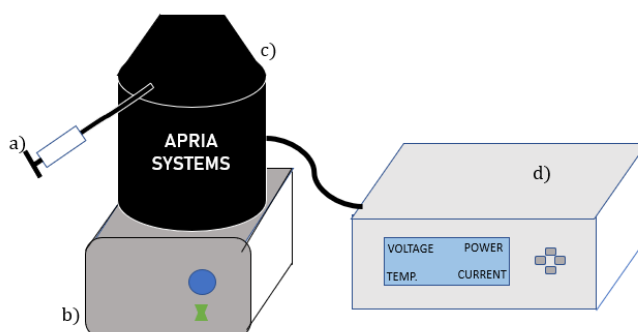


Figure 9. Schematic of photocatalytic assay's system. a) sample collection, b) magnetic stirring plate, c) cylindrical photocatalytic reactor of 1 L of capacity, d) control board

The membranes were placed with the support as in Figure 8. This support, in some photocatalysis assays, did not have proper ventilation due to the lack of holes for ventilation, since the lid of the glass reactor was completely closed, however, when performing other assays already with the definitive support, it was corroborated that there was no alteration of the results with the previous assays.

For the membrane containing $\text{TiO}_2\text{-Ag}$, assays were performed with DBS with an initial concentration of 50 mg/L and 20 mg/L in order to analyze the degradation kinetics of the photocatalyst with respect to the concentration of the contaminant, as well as to see the influence of the reuse of the membrane; with respect to the one containing TiO_2 , assays were only performed with an initial concentration of 50 mg/L; likewise, they were also performed with DCA at an initial concentration of 50 mg/L. The duration of the assays was 6 hours, for which samples were taken at established times with a volume as described in the description of the adsorption methodology. The assays were carried out under the conditions shown in the table 7.

Table 7. Conditions of photocatalysis assays of model pollutants.

Sample	Model contaminant/ C_0 mg/L	Temperature (°C)	pH ₀	Membrane area (cm ²)
TiO ₂	DBS/50	31.9	5.58	29.03
TiO ₂ -Ag	DBS/50	28.1	5.58	30.16
TiO ₂ -Ag	DBS/20	28.3	5.85	30.16
TiO ₂	DCA/50	28.8	3.30	24.12
TiO ₂ -Ag	DCA/50	30	3.38	26.77

3.3.5. Coupled photocatalysis and filtration evaluation

This system is comprised of a combination of photocatalysis and filtration. Therefore, it consists of the membrane placed inside the reactor which in turn is connected to the vacuum trap, and the latter to the vacuum pump (Figure 10). This system was not carried out in automated monitoring; therefore, the flow was calculated according to equation (6). The membrane was placed inside the reactor which contained DCA with a concentration of 50 mg/L; with a temperature of 26.9 ± 1.5 °C and initial pH of 3.38 for the assays with the TiO₂ membrane, whilst the TiO₂-Ag membrane 27.3 ± 1.5 °C and initial pH of 3.50. For this trials, TiO₂ membrane had a membrane area of 24.50 cm² and the TiO₂-Ag membrane 24.13 cm².

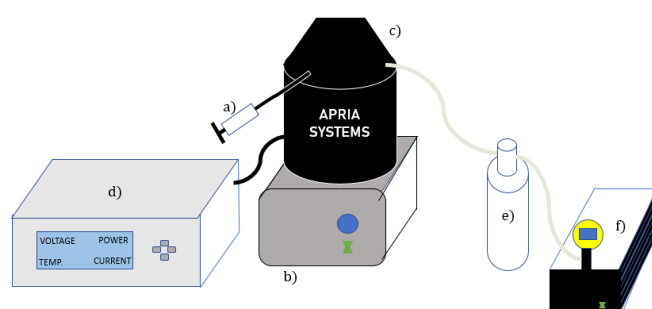


Figure 10. Photocatalysis paired with filtration system. a) sample collection, b) magnetic stirring plate, c) cylindrical photocatalytic reactor of 1 L of capacity, d) control board, e) vacuum trap, f) vacuum pump.

For the operation of this system, a filtration cycle of about 4 minutes for the TiO₂ membrane and 5 minutes for TiO₂-Ag were performed, because the vacuum trap was filled. After this cycle, the vacuum was broken to take the concentration samples of the contaminant in the permeate, that was in the vacuum trap, and in the reactor tank. Once these samples were taken, the permeate collected in the trap were returned to the tank inside the reactor. These assays had a duration of 6 hours; in which UV light did not stop irradiating (Fig. 11). Volume sampling was taken at determined times.

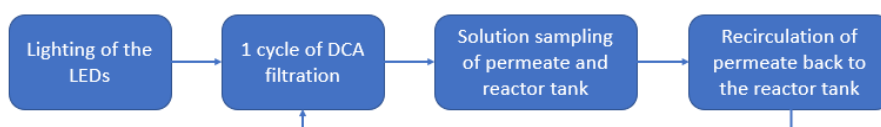


Figure 11. Scheme of the photocatalysis and filtration paired assays

4. RESULTS AND DISCUSSION

Regarding the results, first the water permeability results will be shown, as well as the permeability and filtration of DBS; then the adsorption results will be shown, followed by the photocatalysis experiments and finally the photocatalysis tests coupled with the filtration.

4.1. Permeability tests

In the permeability tests, in the case of zeolite membranes, 2 pieces of membrane belonging to the same sample were tested, so the water flux experiments belonging to the FAU 03 and FAU 06 samples were performed with 2 pieces of different membrane (FAU 03 1, FAU 03 2, FAU 06 1, FAU 06 2); nevertheless, these two pieces were considered as the same sample for the hydraulic permeability calculation. For the hydraulic permeability, the trials at different pressures and the water flux were plotted with a trend line and intercepting the origin.

Regarding the behavior of water flux with increasing differential pressure, the highest flux found for the FAU 03 zeolite membrane is 19.41 L/m²h at a pressure of 1.04 bar, while the lowest flux 2.19 L/m²h at the same pressure. The FAU 06 zeolite membrane has its highest flux with a value of 49.76 L/m²h at a pressure of 0.99 bar; while the lowest is 7.65 L/m²h at 1.046 bar. In spite of the tests at different pressures (Fig. 12), the membranes show a flat trend and taking into account that the range of pressures in which they worked was not so wide apart, it can be assumed that in this range of pressures there is no significant influence on the change in flux.

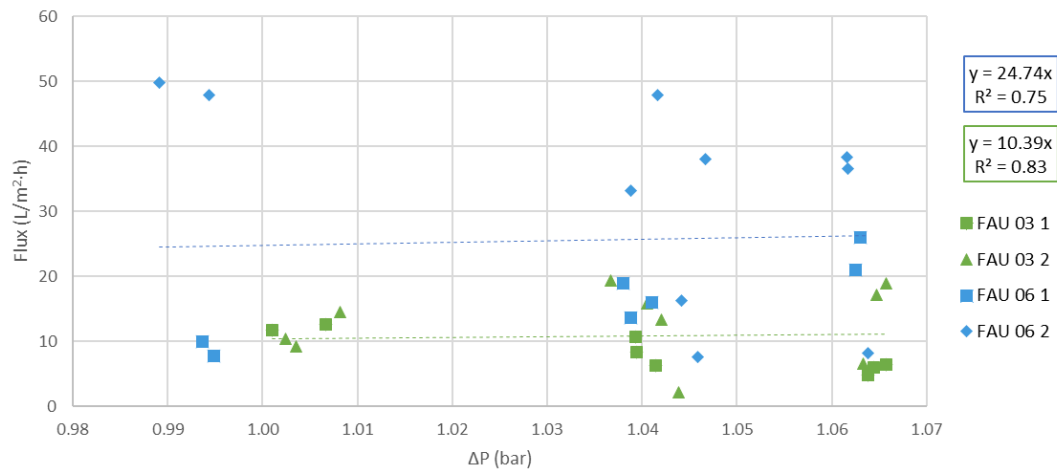


Figure 12. Water flow behavior with increase of ΔP in zeolite membranes.

As for the trials of the change in water flux over time with the TiO_2 and $\text{TiO}_2\text{-Ag}$ membranes, in Figure 13 and 14, and the trend line data were fitted to when at a $\Delta P = 0$, the water flow was also 0; which is in accordance with actual physical behavior. The trend line of both membranes has a slightly positive behavior, even so, it has actually a flat response; thus, reflecting that there is no much influence of the change in pressure in that range.

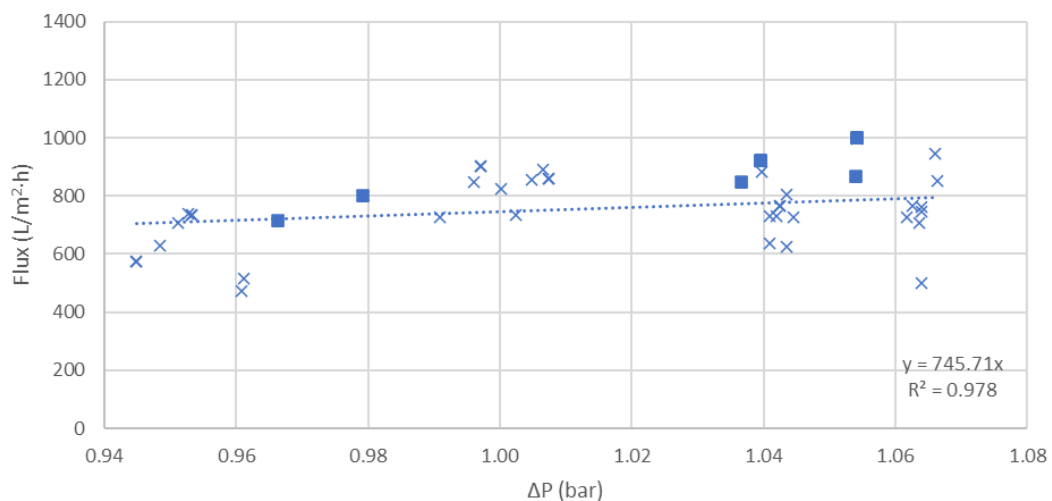


Figure 13. TiO_2 membrane water flow behavior with increase of ΔP .

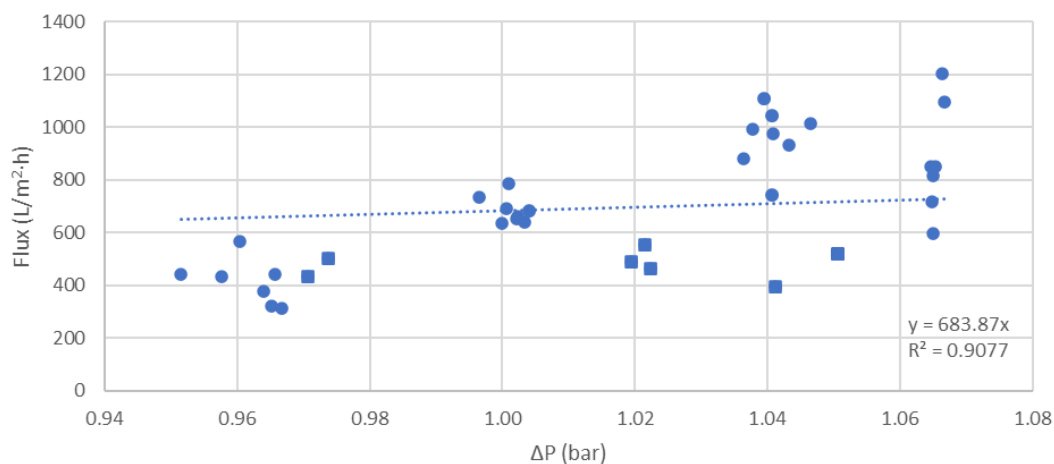


Figure 14. $\text{TiO}_2\text{-Ag}$ membrane water flow behavior with increase of ΔP .

Table 8 shows the permeabilities of the membranes with their corresponding R^2 , Basumatary et al. (2016); synthesized a macroporous ceramic support and a FAU zeolite; to develop a composite membrane that 21.9 $\text{L/m}^2\text{h bar}$; as well Workneh, (2008) manufactured a composite membrane with a homemade clay support and a zeolite active layer; they reported a hydraulic permeability of 270 $\text{L/m}^2\text{h bar}$; also, Vinoth Kumar et al. (2017) made a membrane by coating FAU zeolite on a tubular ceramic support that showed a hydraulic permeability of 58.32 $\text{L/m}^2\text{h bar}$. Comparing the hydraulic permeabilities of the zeolite membranes obtained in this project with those reported by other authors, it can be noted that they are in a similar range; at least for those reported by the authors afore mentioned; it is also important to note that the zeolite membrane FAU 06, which has a higher permeability than FAU 03, has a permeability very close to those reported by the aforementioned authors.

As for the TiO_2 and $\text{TiO}_2\text{-Ag}$ membranes, the hydraulic permeability (Table 13) is very high, compared to the zeolite's one; the TiO_2 membrane has a hydraulic permeability 30 times higher than the FAU 06, whilst the $\text{TiO}_2\text{-Ag}$ membrane 28 times higher; nonetheless, between the both photocatalytic membranes, there is not a big gap in the permeability values. Song et al. (2016) synthesized TiO_2 nanofiltration membranes flat supported by anodic aluminum oxide membranes; with this membrane, they obtained a water permeance of 48 $\text{L/m}^2\text{h bar}$. Ahmad et al. (2017b) developed a composite

membrane of organized mesoporous TiO₂ coated on a porous alumina support, in which they observed a permeability of 20.5 L/m²h bar. Ahmad et al. (2017a) tested a photocatalytic TiO₂ membrane on a flat α -alumina support and reported a 9.9 L/m²h bar hydraulic permeability. In this work, the tested TiO₂ membrane has a hydraulic permeability of 745.71 L/m²h bar and a R² of 0.98, thus, showing a high reliability in the data behavior. Comparing the hydraulic permeability with those reported by other authors, there is a huge gap between the values reported; nonetheless, the permeabilities of the authors mentioned are from type of membranes that are not the same membranes as the ones used in this work, so this may be the reason for the difference; as well, the experimental permeability system of these authors was different from the one used in this work, in the sense that for this project a vacuum pressure was used for the water to permeate through the membrane, while they increased the flow pressure to carry out the filtration.

Ma et al. (2010) developed a membrane with porous α -Al₂O₃ ceramic disk supports embedded with a hydroxyapatite (HPA) and TiO₂-Ag layer, this resulted with an 844.9 L/m²h bar permeability; whilst in this work the TiO₂-Ag membrane has a value of 638.87 L/m²h, and also represents a high fit of the model to the data.

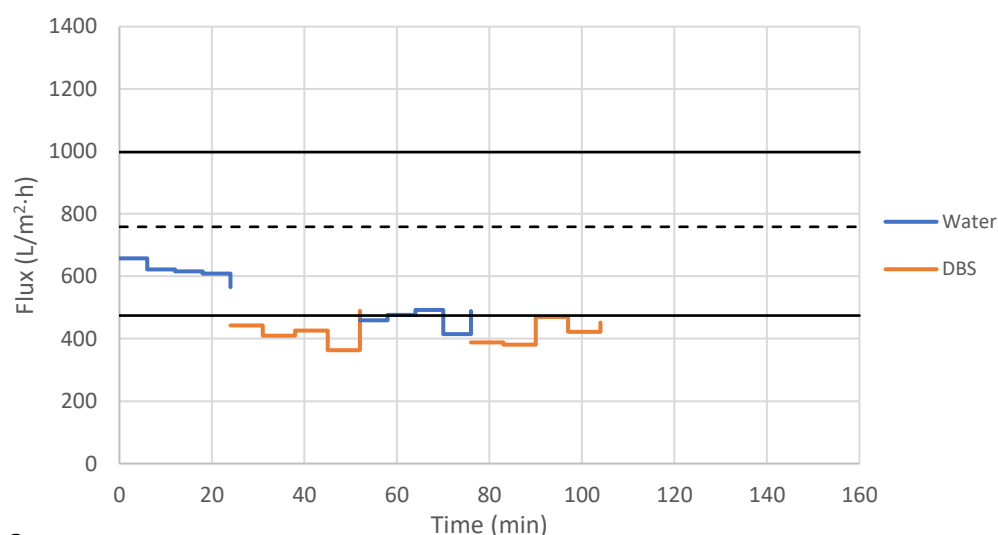
Table 8. Permeability summary.

Sample	Hydraulic permeability L/m ² ·h·bar	R ²
FAU 03	10.39	0.83
FAU 06	24.74	0.75
TiO ₂	745.71	0.98
TiO ₂ -Ag	683.87	0.91

4.1.1. Model compound filtration

In Figure 15 is shown the behavior of the flux of water and DBS over time. In Figure 14a, it can be observed that the TiO₂ membrane in the first water cycles has flux values between 565-657 L/m²h bar, to later, with the DBS filtration, obtain fluxes in ranges between 363-489 L/m²h bar; in the experiment after the DBS, which is the water

experiment, permeabilities between 388-492 L/m²h bar were obtained. In these experiments, it can be observed that after the DBS cycle, in this membrane, the fluxes of the initial water experiment were not recovered. The values of the initial water flux are within the water flux ranges already reported according to the corresponding pressures, nonetheless, the post-DBS water flux experiment is a bit below the lowest hydraulic permeability reported, but this is considered part of experimental error. As for the DBS assays, they slightly fall below the lowest water flux, however, when comparing it to the behavior in Figure 16 and of the membrane TiO₂-Ag, it can also be considered an experimental error. With respect to the TiO₂-Ag membrane, there is a clearer tendency in flux decreasing when DBS is filtered and then increases again when water is permeated. In TiO₂-Ag membrane, practically, all the fluxes are within the range of water flux reported.



a

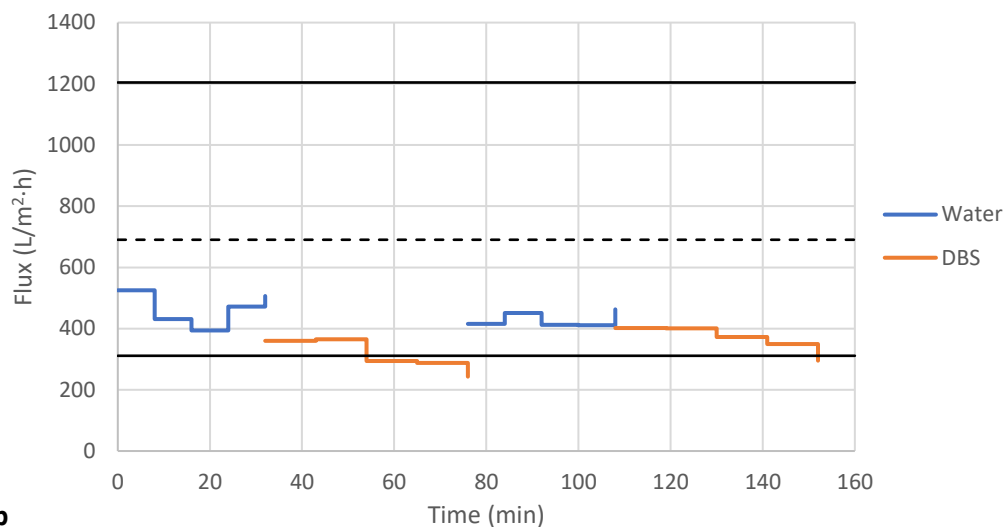


Figure 15. Permeate flux change in 5 filtration cycles; each cycle duration: a) 7 min. TiO_2 membrane, b) 11 min. $\text{TiO}_2\text{-Ag}$ membrane. Flux calculated with permeate mass through time. First 5 cycles with water were performed, followed by DBS cycles and so on (washing in between).

Figure 16 shows the comparison of the permeate fluxes by performing a single water cycle to later evaluate a DBS cycle; in the TiO_2 membrane experiments (Fig. 16a) it can be observed that the DBS fluxes are actually within the range of the water permeabilities of the preliminary tests, which can be translated that there is really no significant change in the permeate flux when DBS is filtered to when water is filtered. Also, it can be observed that in the last water cycle a higher water flux is observed than the water flux obtained in the preliminary water permeability tests; however, this can be attributed to some experimental error.

In the $\text{TiO}_2\text{-Ag}$ tests (Fig. 16b) a slight decrease in DBS fluxes is observed after the water filtration cycles; however, the DBS fluxes are also within the ranges of the hydraulic water permeation tests; therefore, it can be assumed that this membrane also does not have a significant change in flux when water or DBS is permeated; thus, no fouling is present.

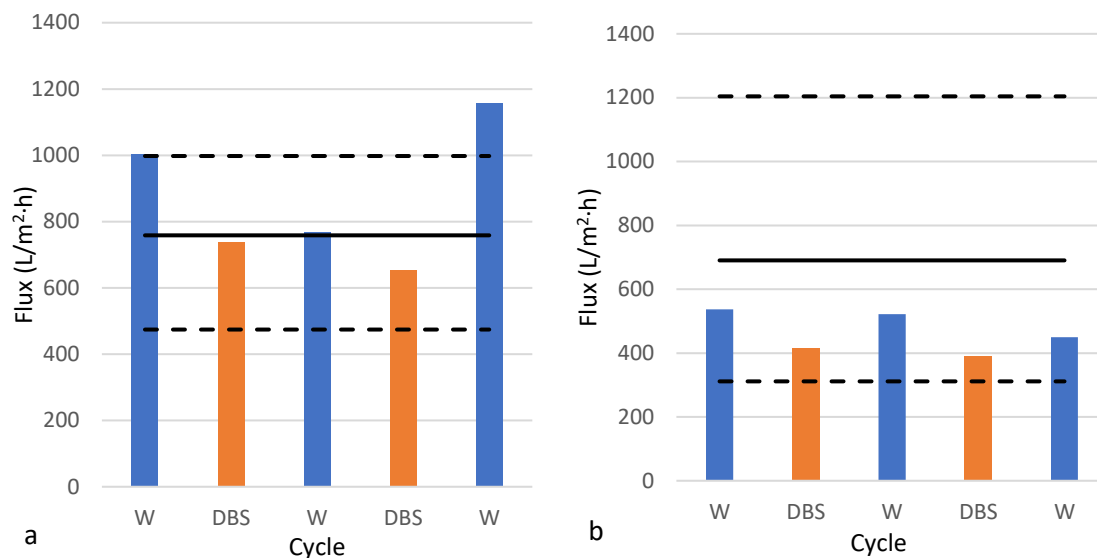


Figure 16. Comparison of permeation flux; interspersed with water and DBS trials. W: Water. (Flux calculated with final volume and time). a) TiO₂ membrane, b) TiO₂-Ag membrane.

Figure 17 shows the changes in DBS concentration due to the filtration of the contaminant; several peaks that go down and up can be observed; this is because the experiments were carried out in cycles, due to limitations with the vacuum trap, so at the beginning and end of each cycle, samples of the DBS concentration were taken to observe its filtration. In Figure 17a it can be observed that in the TiO₂ membrane the change in concentration remained relatively constant; however, the highest percentage of rejection obtained was 2%; the same trend in the graph can be observed for the TiO₂-Ag membrane, also with the highest percentage of rejection of 2%. Thus, it can be assumed, that filtration by itself, for both photocatalytic membranes, do not have a significant impact in DBS decrease of concentration. Workneh, (2008b) showed a rejection of SDS in a range of 10-45% and a hydraulic permeability of 270 L/m²h bar. Zhang et al. (2006) reported a rejection of 60-70% of DBS with silica/titania nanorods/nanotubes composite membrane and a DBS flux of 47 L/m²h at 0.5 bar ΔP . Taking into account the hydraulic permeabilities of TiO₂ and TiO₂-Ag membranes; and their average DBS flux of 696 and 403 L/m²h, respectively, at 0.97 bar, it can be noted that the evaluated membranes follow the usual membrane behavior reported, that is when the flux rises, the rejection capacity decreases (Bae, 2020). Thus, these membranes, with filtration itself, do not present enough rejection capacity for their implementation in water polluted with these substances.

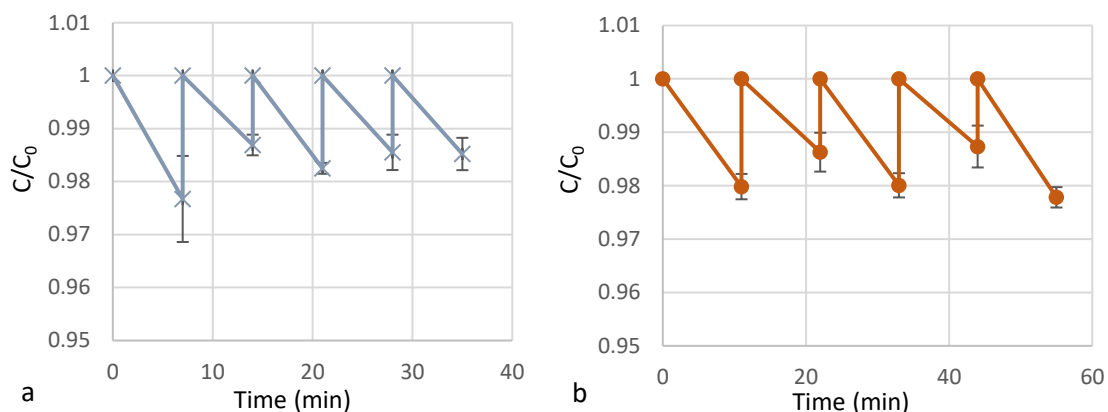


Figure 17. DBS change in concentration through 5 filtration cycles a) each cycle duration: 9 min.; TiO_2 membrane. b) each cycle duration: 17 min.; TiO_2 -Ag membrane. (Flux calculated with final volume and time).

4.2. Adsorption evaluation

In the membrane adsorption tests, at the end of the 120 minutes of testing, a final pH of 6.24 was recorded for the DBS tests with the TiO_2 membrane and 6.20 for the tests with the same contaminant, but with the TiO_2 -Ag membrane; in the case of DCA trials, in the experiments with the TiO_2 membrane a final pH of 3.41 was obtained, while for the TiO_2 -Ag membrane a final pH of 3.43 was obtained; so, comparing the initial pH with the final pH, there was really no significant change between them. Adsorption tests were performed considering that since the membranes are composites of the photocatalyst layer with the zeolite, adsorption could have occurred due to the presence of the zeolites, nonetheless, it was found that the photocatalytic membranes do not adsorb DBS or DCA (Fig. 18). Since the membranes do not adsorb the model contaminants studied, it is assumed that the 2% of rejection in the filtration tests were due to the sieving effect of the membranes due to the presence of zeolites in the membranes.

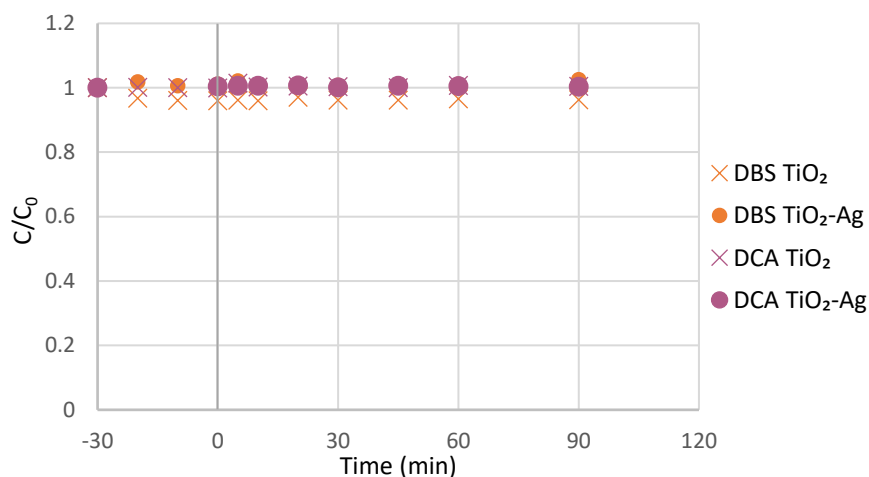


Figure 18. Adsorption of DBS and DCA with TiO₂ and TiO₂-Ag membranes.

4.3. Photocatalytic evaluation

In the photocatalysis tests, the final pH data were recorded; in the DBS tests with the TiO₂ membrane, a pH of 3.98 was obtained, while in the TiO₂-Ag membrane in the DBS tests with an initial concentration of 50 mg/L, a final pH of 4.48 was obtained, while in the tests with initial concentration of 20 mg/L a pH of 4.3. This pH reduction can be attributed to the formation of intermediate organic compounds such as short chain organic acids. With respect to the DCA test with the TiO₂ membrane, a final pH of 3.22 was obtained and with the TiO₂-Ag membrane a pH of 3.25. Therefore, pH variation is negligible.

Photocatalysis tests (Fig. 19) show that the TiO₂-Ag membrane, for both pollutants, has a higher percentage of degradation than TiO₂. The TiO₂ membrane had a degradation percentage of 16.6% of DBS, 37% of DCA, while TiO₂-Ag 21% of DBS and 44% of DCA. Other authors, like Zhang et al. (2006) report DBS degradation percentages of approximately 50% when using a silica/titania nanorods/nanotubes composite membrane. Although the membrane areas varied between the two membranes and between tests with the two contaminants, the same linear degradation trend can be seen for both contaminants. The increase in pollutant degradation with the TiO₂-Ag membrane may be due to the fact that Ag decreases the rate of electron/hole recombination (Shi et al., 2017).

In Figure 19 it can also be observed that the experimental data follow very closely the simulation data. Therefore, the experimental data are in agreement with the degradation data according to the proposed kinetic model. Data was adjusted to a 0-order kinetic model. It was also proven the independence of the degradation speed from the initial concentration of the pollutants (Fig. 20). Therefore, it can be deduced that the degradation rate is not affected by the concentration of the pollutant, in the conditions of this work.

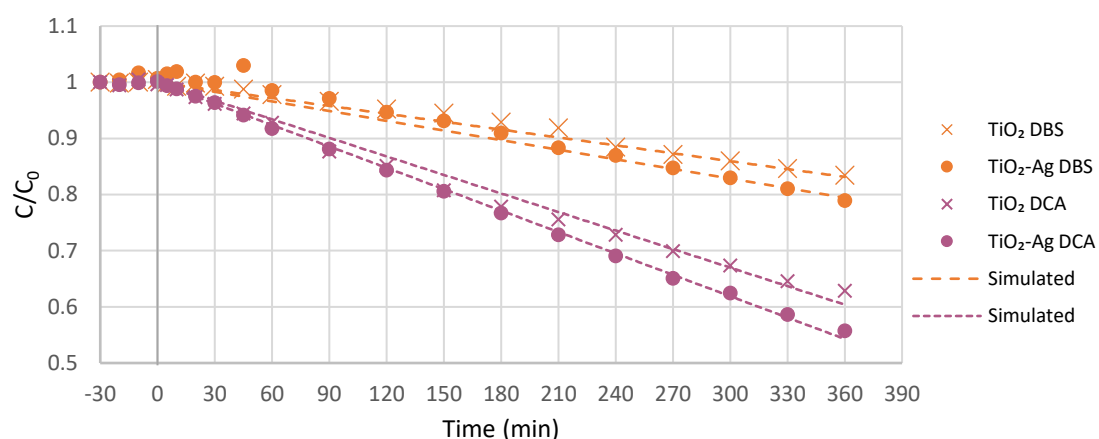


Figure 19. Experimental photocatalytic degradation and simulation of DBS and DCA with TiO_2 and TiO_2 -Ag membranes. Simulated data with zero-order kinetic model.

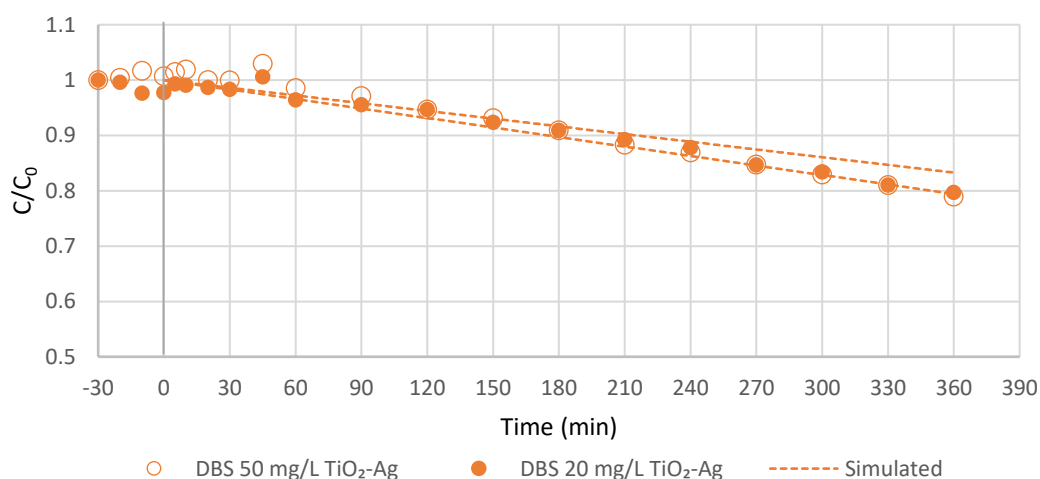


Figure 20. Experimental photocatalytic degradation and simulation of DBS at an initial concentration of 20 mg/L and 50 mg/L with TiO_2 -Ag membrane.

Although usually in photocatalysis there are pseudo first order kinetics, the data obtained experimentally showed that the data fitted a kinetic model of order 0. The R^2

of each experiment shows that this model represents very accurately the kinetics in this work (Table 9). Likewise, the highest kinetic rate constant (k) is that of the TiO₂-Ag membrane with the DCA assays.

Table 9. Kinetic constant of different trials and its correspondent coefficient of determination

Trial	Compound	k (mg/L·min)	R ²
TiO ₂	DBS	0.024	0.995
	DCA	0.052	0.996
TiO ₂ -Ag	DBS 50	0.029	0.981
	DBS 20	0.009	0.952
	DCA	0.062	1.000

4.4. Coupled photocatalysis and filtration evaluation.

In the coupled photocatalysis and filtration tests, the trend of the fluxes was observed, as well as the DCA concentrations in the permeate and in the reactor (Fig. 21). The TiO₂-Ag membrane was found to have a slightly higher percentage of degradation and retention. However, the flux does have a slight decay; while in the TiO₂ membrane the flux remains relatively constant TiO₂ membrane; also, it has a total decrease of 59% in DCA concentration, while the TiO₂-Ag of 67%. Unlike the photocatalysis alone tests, the trend in the decrease of DCA concentration is more curved. The reactor and permeate concentrations were taken separately to observe the individual influence of both processes when coupled. It can be observed that in these tests the filtration did not have an influence on the decrease in DCA concentration. The reason why in the permeate there is more DCA concentration than in the reactor tank at the same sampling time, is because while filtering, the solution that remains inside the tank, which has a minor quantity than the initial one, is still irradiated by light, whereas the filtered one is not. Thus, permeate data would be the average of the concentration data from the prior and final time points.

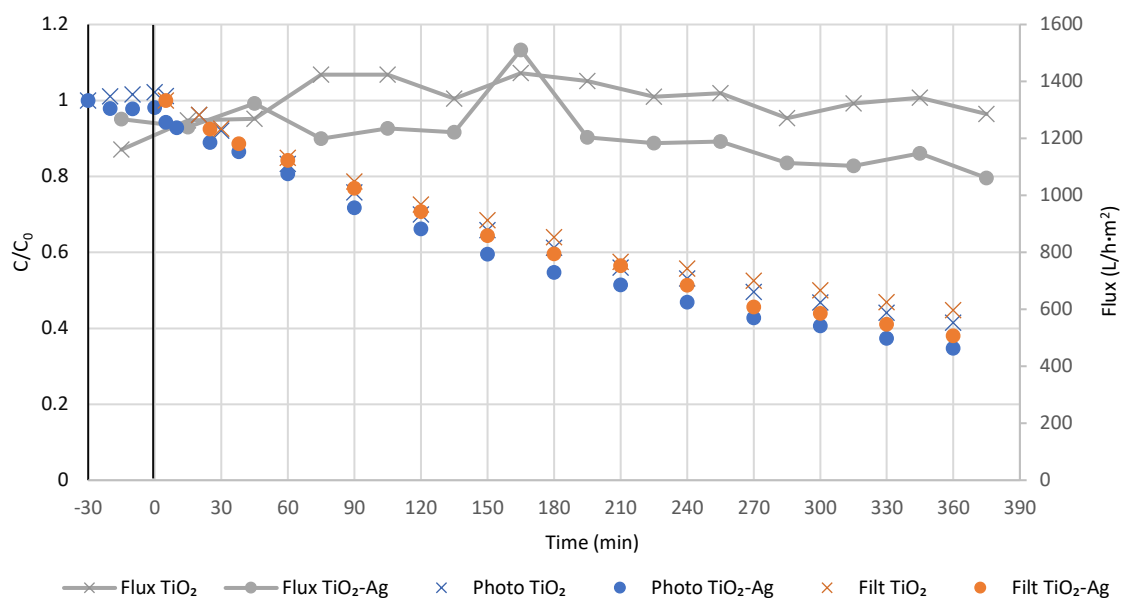


Figure 21. Photocatalysis paired with filtration of DCA with TiO_2 and $\text{TiO}_2\text{-Ag}$ membranes. Photo: Concentration of DCA at reactor tank, Filt: Concentration of DCA at permeate.

Figures 22 and 23 show the results obtained in the coupled photocatalysis and filtration experiments compared to the degradation results obtained without the combination of both techniques for TiO_2 and $\text{TiO}_2\text{-Ag}$ membranes, respectively. The graphs show the simulation of the concentration behavior according to the kinetics. While in the photocatalysis alone tests, the data were fitted to a 0-order kinetics model, in the case of the coupled photocatalysis and filtration tests, the data were adjusted to a 1-order kinetics model. In the TiO_2 membrane, a k of 0.0027 1/min with an R^2 of 0.99 was obtained. The $\text{TiO}_2\text{-Ag}$ membrane had a k of 0.003 1/min and R^2 of 1. In the TiO_2 membrane the percentage of degradation with both systems coupled is 1.6 times greater than that of photocatalysis alone; while that of the $\text{TiO}_2\text{-Ag}$ membrane is 1.5 times greater.

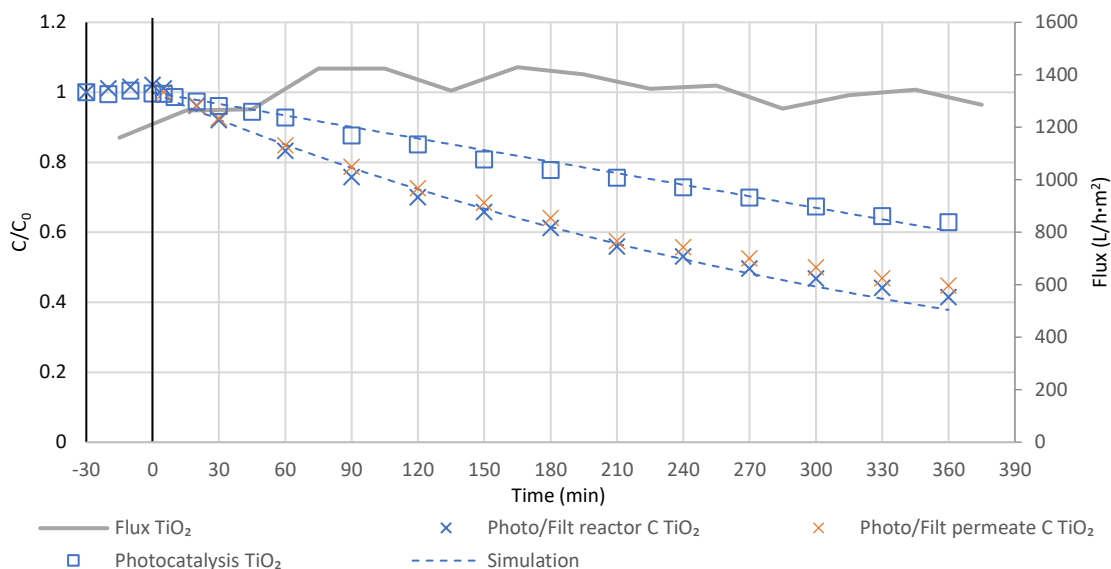


Figure 22. Comparison of change in concentration of photocatalysis trial and photocatalysis paired with filtration trial of DCA with TiO_2 membrane. Photo/Filt reactor C: change in concentration of DCA at reactor tank, Photo/Filt permeate C: change in concentration of DCA at permeate.

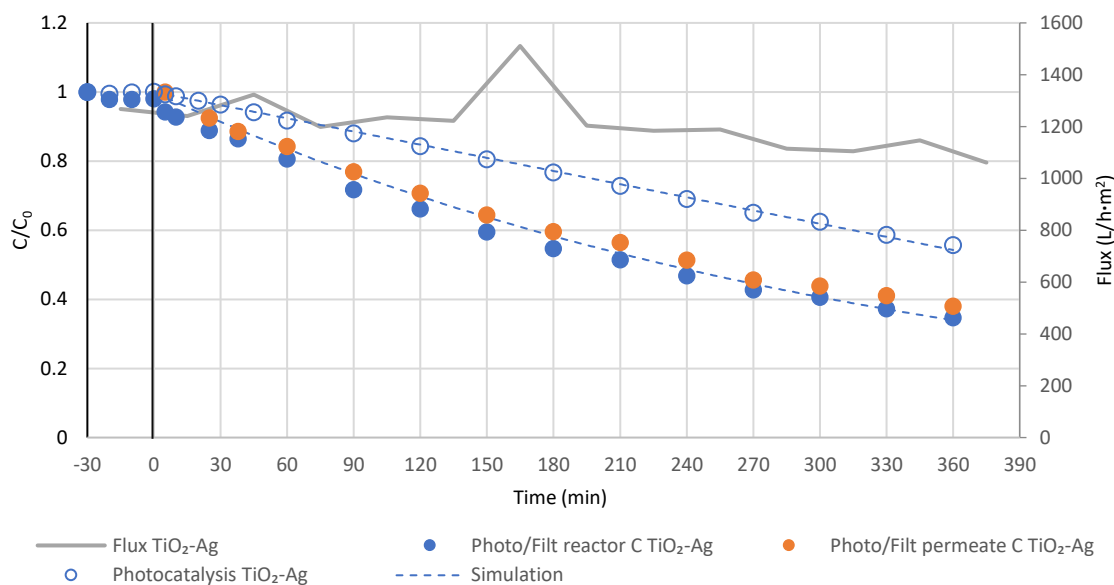


Figure 23. Comparison of change in concentration of photocatalysis trial and photocatalysis paired with filtration trial of DCA with TiO_2-Ag membrane. Photo/Filt reactor C: change in concentration of DCA at reactor tank, Photo/Filt permeate C: change in concentration of DCA at permeate.

As for the results presented, it can be observed that there is synergy in coupled filtration photocatalysis, that favors DCA degradation. It should also be noted that in all the photocatalysis tests there was an improvement in the degradation of the model pollutants with the TiO_2-Ag membrane. This trend was not present with the filtration tests, since the results of the two membranes were practically the same.

The decrease in concentration in the photocatalysis and coupled filtration system cannot be attributed to the rejection of DCA by the membrane because in the DBS filtration tests practically no rejection was observed. Therefore, since DCA is a smaller molecule than DBS, it will not be rejected by the membrane either. The increase in the degradation of DCA can be attributed to the fact that there are oxidizing species that in the photocatalysis system alone do not interact with the pollutant. When coupling photocatalysis and filtration, by forcing the contaminant through the membrane, it may interact with oxidant species that have formed in the inner layers of the membrane. This is because there may be photocatalyst within the zeolite structure, which being UV transparent, causes oxidative species to be generated within the zeolite structure, which are not available for contaminant degradation unless the contaminant passes through the zeolite structure. The deposition of the photocatalyst inside the zeolite structure depends on the concentration of the photocatalyst with which the membrane has been prepared, since if a very large amount is used, it is difficult for the particles to enter the zeolite structure (Lavorato et al., 2017). However, this study is outside the scope of this project, so it would be interesting to evaluate it in the future. The increase in DCA degradation performance, can also be due to the fact that when h^+ are generated (that do not diffuse in the solution), these can either directly react with organic compounds (Fujishima et al., 2008) or react with adsorbed water or adsorbed hydroxides (OH^-), thus forming adsorbed (OH^-_{ads}) (Vital-Grappin et al., 2021). These OH^-_{ads} could be close to the membranes, thus, only available when the pollutant passes through the membrane, and has contact with these reactive species.

5. CONCLUSIONS

According to the results obtained and already discussed, it can be concluded that:

- Zeolite membranes exhibit a hydraulic permeability similar to that reported with other authors; and photocatalytic membranes present about 30-fold more hydraulic permeability.
- Regarding filtration as a separate treatment, DBS is not removed by the membranes used in this work, and photocatalytic membranes have no adsorption properties for DBS and DCA.
- After 6h photocatalytic DCA degradation reached 37% with TiO_2 and 44% with $\text{TiO}_2\text{-Ag}$, and DBS removal of 16% and 21%, was achieved with both catalysts respectively. Therefore, the presence of Ag in the PMs does improve the DCA and DBS degradation, due to the decrease in electron/hole recombination rate.
- When coupling filtration and photocatalysis, after 6h DCA removal was 59% for TiO_2 and 67% for $\text{TiO}_2\text{-Ag}$ due to higher contact between the contaminants and the oxidative reactive species.
- The experimental results fitted to a 0-order kinetic model of photocatalysis when embedded into the membrane. When coupling photocatalysis and filtration, data fitted to a 1-order kinetics model. Therefore, due to the pollutant's excess at the evaluated concentrations and the lack of any constraints on the pollutant's diffusion near the catalyst surface, the system is limited by the production of reactive oxygen species.

Further work should also consider the evaluation of DBS concentration change with coupled photocatalysis and filtration. As well, it would be of interest to assess the filtration and degradation of contaminants with bigger molecules, such as, humic acids.

6. NOMENCLATURE

AOP	Advanced Oxidation Process
C	Concentration at time t
C ₀	Initial concentration
CO ₂	Carbon dioxide
DBS	Sodium dodecyl benzene sulfonate
DCA	Dichloroacetic acid
EP	Emerging pollutants
FAU	Faujite zeolite
HCO ₃ ⁻	Bicarbonate
H ₂ O	Water
H ⁺	Hydron
k	Kinetic rate constant
mg/L	Unit of concentration
mW/cm ²	Irradiance unit
P _r	Reference pressure
P _v	Vacuum pressure
R ²	Regression coefficient (0 < R ² < 1)
TiO ₂	Titanium dioxide
TiO ₂ -Ag	Titanium dioxide doped with silver
UV	Ultraviolet radiation
ΔP	Pressure difference
%R	Rejection percentage

7. BIBLIOGRAPHY

Abbad, S., Guergouri, K., Gazaout, S., Djebabra, S., Zertal, A., Barille, R., Zaabat, M., 2020. Effect of silver doping on the photocatalytic activity of TiO₂ nanopowders synthesized by the sol-gel route. *Journal of Environmental Chemical Engineering*. Vol. 8, no. 3, pp. 103718. DOI 10.1016/J.JECE.2020.103718.

Ahmad, R., Kim, J.K., Kim, J.H., Kim, J., 2017a. Nanostructured Ceramic Photocatalytic Membrane Modified with a Polymer Template for Textile Wastewater Treatment. *Applied Sciences*. Vol. 7, no. 12, pp. 1284. DOI 10.3390/APP7121284.

Ahmad, R., Kim, J.K., Kim, J.H., Kim, J., 2017b. Well-organized, mesoporous nanocrystalline TiO₂ on alumina membranes with hierarchical architecture: Antifouling and photocatalytic activities. *Catalysis Today*. Vol. 282, pp. 2. DOI 10.1016/J.CATTOD.2016.03.051.

Alias, S.S., Harun, Z., Latif, I.S.A., 2018. Characterization and performance of porous photocatalytic ceramic membranes coated with TiO₂ via different dip-coating routes. *Journal of Materials Science*. Vol. 53, no. 16, pp. 11534. DOI 10.1007/S10853-018-2392-3/FIGURES/7.

Ameta, R., Solanki, M.S., Benjamin, S., Ameta, S.C., 2018. Photocatalysis. *Advanced Oxidation Processes for Wastewater Treatment: Emerging Green Chemical Technology*. pp. 135. DOI 10.1016/B978-0-12-810499-6.00006-1.

Assadi, Y., Farajzadeh, M.A., Bidair, A., 2012. Dispersive Liquid–Liquid Microextraction. In: *Comprehensive Sampling and Sample Preparation*. Elsevier. pp. 181.

Athanasekou, C.P., Romanos, G.E., Katsaros, F.K., Kordatos, K., Likodimos, V., Falaras, P., 2012. Very efficient composite titania membranes in hybrid ultrafiltration/photocatalysis water treatment processes. *Journal of Membrane Science*. Vol. 392, pp. 192. DOI 10.1016/J.MEMSCI.2011.12.028.

Athanasekou, C.P., Moustakas, N.G., Morales-Torres, S., Pastrana-Martínez, L.M., Figueiredo, J.L., Faria, J.L., Silva, A.M.T., Dona-Rodríguez, J.M., Romanos, G.E., and Falaras, P., 2015. Ceramic photocatalytic membranes for water filtration under UV and visible light. *Applied Catalysis B: Environmental*. Vol. 178, pp. 12. DOI 10.1016/J.APCATB.2014.11.021.

Bae, W., Kim, J., 2020. Permeate Flux and Rejection Behavior in Submerged Direct Contact Membrane Distillation Process Treating a Low-Strength Synthetic Wastewater. *Applied Sciences*. Vol. 10, no. 2, pp. 677. DOI 10.3390/APP10020677.

Basumatary, A.K., Kumar, R. V., Ghoshal, A.K., Pugazhenth, G., 2016. Cross flow ultrafiltration of Cr(VI) using MCM-41, MCM-48 and Faujasite (FAU) zeolite-ceramic composite membranes. *Chemosphere*. Vol. 153, pp. 436. DOI 10.1016/j.chemosphere.2016.03.077.

Bautista-Toledo, M.I., Rivera-Utrilla, J., Méndez-Díaz, J.D., Sánchez-Polo, M., Carrasco-Marín, F., 2014. Removal of the surfactant sodium dodecylbenzenesulfonate from water by processes based on adsorption/bioadsorption and biodegradation. *Journal of Colloid and Interface Science*. Vol. 418, pp. 113. DOI 10.1016/J.JCIS.2013.12.001.

Beltrán, F.J., García-Araya, J.F., Álvarez, P.M., 2000. Sodium Dodecylbenzenesulfonate Removal from Water and Wastewater. 1. Kinetics of Decomposition by Ozonation. *Industrial & Engineering Chemistry Research*. Vol. 39, no. 7, pp. 2214. DOI 10.1021/ie990721a.

Beltrán-Heredia, J., Sánchez-Martín, J., Solera-Hernández, C., 2009. Removal of sodium dodecyl benzene sulfonate from water by means of a new tannin-based coagulant: Optimisation studies through design of experiments. *Chemical Engineering Journal*. Vol. 153, no. 1, pp. 56. DOI 10.1016/j.cej.2009.06.012.

Berger, T.E., Regmi, C., Schäfer, A.I. and Richards, B.S., 2020. Photocatalytic degradation of organic dye via atomic layer deposited TiO₂ on ceramic membranes in single-pass flow-through operation. *Journal of Membrane Science*. Vol. 604, pp. 118015. DOI 10.1016/J.MEMSCI.2020.118015.

Bhandari, P.S., Gogate, P.R., 2019. Microwave assisted persulfate induced degradation of sodium dodecyl benzene sulfonate. *Korean Journal of Chemical Engineering*. Vol. 36, no. 12, pp. 2000. DOI 10.1007/s11814-019-0390-z.

Boussu, K., Kindts, C., Vandecasteele, C., Van Der Bruggen, B., 2007. Surfactant Fouling of Nanofiltration Membranes: Measurements and Mechanisms. *ChemPhysChem*. 2007. Vol. 8, no. 12, pp. 1836. DOI 10.1002/cphc.200700236.

Bradai, M., Han, J., Omri, A.E., Funamizu, N., Sayadi, S., Isoda, H., 2016. Effect of linear alkylbenzene sulfonate (LAS) on human intestinal Caco-2 cells at non cytotoxic concentrations. *Cytotechnology*. Vol. 68, no. 4, pp. 1267. DOI 10.1007/s10616-015-9887-4.

BRITANNICA, 2022. Surfactant | Definition, Properties, Examples, & Facts. <https://www.britannica.com/science/surfactant>. 4 May 2022.

Buonomenna, M.G., 2016. Smart composite membranes for advanced wastewater treatments. *Smart Composite Coatings and Membranes: Transport, Structural, Environmental and Energy Applications*. pp. 371. DOI 10.1016/B978-1-78242-283-9.00014-2.

Caro, J., Noack, M., 2008. Zeolite membranes – Recent developments and progress. *Microporous and Mesoporous Materials*. Vol. 115, no. 3, pp. 215. DOI 10.1016/j.micromeso.2008.03.008.

Chakhtouna, H., Benzeid, H., Zari, N., Qaiss, A.E., Bouhfid, R., 2021. Recent progress on Ag/TiO₂ photocatalysts: photocatalytic and bactericidal behaviors. *Environmental Science and Pollution Research*. Vol. 28, no. 33, pp. 44638. DOI 10.1007/S11356-021-14996-Y.

Chao, H.E., Yun, Y.U., Xingfang, H.U., Larbot, A., 2003. Effect of silver doping on the phase transformation and grain growth of sol-gel titania powder. *Journal of the European Ceramic Society*. Vol. 23, no. 9, pp. 1457. DOI 10.1016/S0955-2219(02)00356-4.

Chen, J.P., Mou, H., Wang, L.K, Matsuura, T., 2006. Membrane Filtration. *Advanced Physicochemical Treatment Processes*. pp. 203. DOI 10.1007/978-1-59745-029-4_7.

Choi, H., Stathatos, E., Dionysiou, D.D., 2006. Sol-gel preparation of mesoporous photocatalytic TiO₂ films and TiO₂/Al₂O₃ composite membranes for environmental applications. *Applied Catalysis B: Environmental*. Vol. 63, no. 1, pp. 60. DOI 10.1016/J.APCATB.2005.09.012.

Clara, M., Scharf, S., Scheffknecht, C. And Gans, O., 2007. Occurrence of selected surfactants in untreated and treated sewage. *Water Research*. Vol. 41, no. 19, pp. 4339. DOI 10.1016/j.watres.2007.06.027.

COMISIÓN NACIONAL DEL AGUA, 2021. Situación del Subsector Agua Potable, Alcantarillado y Saneamiento, edición 2021. *Secretaría de Medio Ambiente y Recursos Naturales*. <https://www.gob.mx/conagua/documentos/situacion-del-subsector-agua-potable-drenaje-y-saneamiento> 28 June 2022

Derbe, T., Temesgen, S., Bitew, M., 2021. A Short Review on Synthesis, Characterization, and Applications of Zeolites. *Advances in Materials Science and Engineering*. Vol. 2021, pp. 1. DOI 10.1155/2021/6637898.

Diban, N., Athes, V., Bes, M., Souchon, I., 2008. Ethanol and aroma compounds transfer study for partial dealcoholization of wine using membrane contactor. *Journal of Membrane Science*. Vol. 311, no. 1, pp. 136. DOI 10.1016/J.MEMSCI.2007.12.004.

Diban, N., Haimi, S., Bolhuis-Versteeg, L., Teixeira, S., Miettinen, S., Poot, A., Grijpma, D., Stamatialis, D., 2013a. Hollow fibers of poly(lactide-co-glycolide) and poly(ϵ -caprolactone) blends for vascular tissue engineering applications. *Acta Biomaterialia*. Vol. 9, no. 5, pp. 6450. DOI 10.1016/J.ACTBIO.2013.01.005.

Diban, N., Haimi, S., Bolhuis-Versteeg, L., Teixeira, S., Miettinen, S., Poot, A., Grijpma, D., Stamatialis, D., 2013b. Development and characterization of poly(ϵ -caprolactone) hollow fiber membranes for vascular tissue engineering. *Journal of Membrane Science*. Vol. 438, pp. 29. DOI 10.1016/J.MEMSCI.2013.03.024.

Diban, N., Pacuła, A., Kumakiri, I., Barquín, C., Rivero, M.J., Urtiaga, A., Ortiz, I., 2021. TiO₂-Zeolite Metal Composites for Photocatalytic Degradation of Organic Pollutants in Water. *Catalysts*. Vol. 11, no. 11, pp. 1367. DOI 10.3390/CATAL11111367.

Diban, N., Urtiaga, A., Ortiz, I., 2008. Recovery of key components of bilberry aroma using a commercial pervaporation membrane. *Desalination*. Vol. 224, no. 1, pp. 34. DOI 10.1016/J.DESAL.2007.04.076.

Dichloroacetic acid | CHCl₂COOH - PubChem, no date. <https://pubchem.ncbi.nlm.nih.gov/compound/Dichloroacetic-acid> 29 June 2022.

Dichloroacetic acid: Uses, Interactions, Mechanism of Action | DrugBank Online, no date. <https://go.drugbank.com/drugs/DB08809> 29 June 2022.

Dominguez, S., Ribao, P., Rivero, M.J., Ortiz, I., 2015. Influence of radiation and TiO₂ concentration on the hydroxyl radicals generation in a photocatalytic LED reactor. Application to dodecylbenzenesulfonate degradation. *Applied Catalysis B: Environmental*. Vol. 178, pp. 165. DOI 10.1016/J.APCATB.2014.09.072.

Duan, Z., Huang, Y., Zhang, D., Chen, S., 2019. Electrospinning Fabricating Au/TiO₂ Network-like Nanofibers as Visible Light Activated Photocatalyst. *Scientific Reports*. Vol. 9, no. 1, pp. 1. DOI 10.1038/s41598-019-44422-w.

Dubey, N., Pal, A., 2012. Micellar solubilization of octan-1-ol in aqueous solutions of SDBS and TTAB. *Journal of Molecular Liquids*. Vol. 172, pp. 12. DOI 10.1016/j.molliq.2012.04.011.

Dzinun, H., Othman, M.H.D., Ismail, A.F., 2019. Photocatalytic performance of TiO₂/Clinoptilolite: Comparison study in suspension and hybrid photocatalytic membrane reactor. *Chemosphere*. Vol. 228, pp. 241. DOI 10.1016/J.CHEMOSPHERE.2019.04.118.

Eccles, H., 1997. Ion exchange - future challenges/opportunities in environmental clean-up. *Progress in Ion Exchange*. pp. 245. DOI 10.1533/9781845698652.4.244.

Ehalt Macedo, H., Lehner, B., Nicell, J., Grill, G., Li, J., Limtong, A., Shakya, R., 2022. Distribution and characteristics of wastewater treatment plants within the global river network. *Earth System Science Data*. Vol. 14, no. 2, pp. 559. DOI 10.5194/essd-14-559-2022.

EPA ORD NCEA INTEGRATED RISK INFORMATION SYSTEM, Us, 2003. TOXICOLOGICAL REVIEW OF DICHLOROACETIC ACID In Support of Summary Information on the Integrated Risk Information System (IRIS). Online. www.epa.gov/iris 29 June 2022.

EUROSTAT, 2022a. Water exploitation index, plus. <https://www.pwc.es/es/publicaciones/energia/assets/gestion-agua-2018-espana.pdf>. 29 June 2022.

EUROSTAT, 2022b. Population connected to urban wastewater collecting and treatment systems, by treatment level. <https://ec.europa.eu/eurostat/databrowser/view/ten00020/default/table?lang=en>. 29 June 2022.

Ferreiro, C., Villota, N., Lombraña, J.I., Rivero, M.J., 2019. An efficient catalytic process for the treatment of genotoxic aniline wastewater using a new granular activated carbon-supported titanium dioxide composite. *Journal of Cleaner Production*. Vol. 228, pp. 1282. DOI 10.1016/J.JCLEPRO.2019.04.198.

Fujishima, A., Zhang, X., Tryk, D.A., 2008. TiO₂ photocatalysis and related surface phenomena. *Surface science reports*. Vol. 63, no 12, p. 515. DOI 10.1016/j.surfrep.2008.10.001.

Fukahori, S., Ichiura, H., Kitaoka, T., Tanaka, H., 2003. Photocatalytic decomposition of bisphenol A in water using composite TiO₂-zeolite sheets prepared by a papermaking technique. *Environmental Science and Technology*. Vol. 37, no. 5, pp. 1048. DOI 10.1021/ES0260115/ASSET/IMAGES/LARGE/ES0260115F00005.JPEG.

Garcia, M.T., Campos, E., Marsal, A., Ribosa, I., 2008. Fate and effects of amphoteric surfactants in the aquatic environment. *Environment International*. Vol. 34, no. 7, pp. 1001. DOI 10.1016/j.envint.2008.03.010.

Geissen, S.U., Xi, W., Weidemeyer, A., Vogelpohl, A., Bousselmi, L., Ghrabi, A., Ennabli, A., 2001. Comparison of suspended and fixed photocatalytic reactor systems. *Water Science and Technology*. Vol. 44, no. 5, pp. 245. DOI 10.2166/wst.2001.0297.

Geissen, V., Mol, H., Klumpp, E., Umlauf, G., Nadal, M., Van Der Ploeg, M., Van De Zee, S.E.A.T.M., Ritsema, C.J., 2015. Emerging pollutants in the environment: A challenge for water

resource management. *International Soil and Water Conservation Research*. Vol. 3, no. 1, pp. 57. DOI 10.1016/j.iswcr.2015.03.002.

Gu, Y., Qiu, Y., Hua, X., Shi, Z., Li, A., Ning, Y., Liang, D., 2021. Critical biodegradation process of a widely used surfactant in the water environment: dodecyl benzene sulfonate (DBS). *RSC Advances*. Vol. 11, no. 33, pp. 20303. DOI 10.1039/D1RA02791C.

Guo, H., Zhao, S., Wu, X., Qi, H., 2018. Fabrication and characterization of TiO₂/ZrO₂ ceramic membranes for nanofiltration. *Microporous and Mesoporous Materials*. Vol. 260, pp. 125. DOI 10.1016/J.MICROMESO.2016.03.011.

Huang, M., Yu, J., Li, B., Deng, C., Wang, L., Wu, W., Dong, L., Zhang, F., Fan, M., 2015. Intergrowth and coexistence effects of TiO₂-SnO₂ nanocomposite with excellent photocatalytic activity. *Journal of Alloys and Compounds*. Vol. 629, pp. 55. DOI 10.1016/j.jallcom.2014.11.225.

IARC, 2014. Trichloroethylene, Tetrachloroethylene, and Some Other Chlorinated Agents. *IARC Monographs on the Evaluation of Carcinogenic Risks to Humans*. 2014. Vol. 106, no. IARC Monographs on the Evaluation of Carcinogenic risks to humans, pp. 219.

INSTITUTO NACIONAL DE ESTADÍSTICA, 2018. Estadística sobre el suministro y saneamiento del agua. https://www.ine.es/dyngs/INEbase/es/operacion.htm?c=Estadistica_C&cid=1254736176834&menu=ultiDatos&idp=1254735976602 . 17 May 2022.

Ivanković, T., Hrenović, J., 2010. Surfactants in the Environment. *Archives of Industrial Hygiene and Toxicology*. Vol. 61, no. 1, pp. 95. DOI 10.2478/10004-1254-61-2010-1943.

Jones, E.R., Van Vliet, M.T.H., Qadir, M., Bierkens, M.F.P., 2021. Country-level and gridded estimates of wastewater production, collection, treatment and reuse. *Earth System Science Data*. Vol. 13, no. 2, pp. 237. DOI 10.5194/essd-13-237-2021.

Khulbe, K.C., Matsuura, T., 2018. Removal of heavy metals and pollutants by membrane adsorption techniques. *Applied Water Science*. Vol. 8, no. 1, pp. 19. DOI 10.1007/s13201-018-0661-6.

Kim, S., Park, C., 2021. Potential of ceramic ultrafiltration membranes for the treatment of anionic surfactants in laundry wastewater for greywater reuse. *Journal of Water Process Engineering*. Vol. 44, pp. 102373. DOI 10.1016/j.jwpe.2021.102373.

Kissling, G.E., Malarkey, D.E., Vallant, M.K., Johnson, J.D., Hejtmancik, M.R., Herbert, R.A. And Boorman, G.A., 2009. Evaluation of Dichloroacetic Acid for Carcinogenicity in Genetically Modified Tg.AC Hemizygous and p53 Haploinsufficient Mice. *Toxicological Sciences*. Vol. 107, no. 1, pp. 19. DOI 10.1093/TOXSCI/KFN228.

Kotobuki, M., Gu, Q., Zhang, L., Wang, J., 2021. Ceramic-Polymer Composite Membranes for Water and Wastewater Treatment: Bridging the Big Gap between Ceramics and Polymers. *Molecules*. Vol. 26, no. 11. DOI 10.3390/MOLECULES26113331.

Kotrotsiou, O., Kiparissides, C., 2019. Water Treatment by Molecularly Imprinted Materials. *Nanoscale Materials in Water Purification*. pp. 179. DOI 10.1016/B978-0-12-813926-4.00012-4.

Król, M., 2020. Natural vs. Synthetic Zeolites. *Crystals*. Vol.10, no. 7, pp.622. DOI 10.3390/cryst10070622.

Kumakiri, I., Hashimoto, K., Nakagawa, Y., Inoue, Y., Kanehiro, Y., Tanaka, K., Kita, H., 2014. Application of FAU zeolite membranes to alcohol/acrylate mixture systems. *Catalysis Today*. Vol. 236, pp. 86. DOI 10.1016/j.cattod.2013.11.064.

Kurrer, C., 2021. Water Protection and Management | Fact Sheets on the European Union | European Parliament. <https://www.europarl.europa.eu/factsheets/en/sheet/74/water-protection-and-management>. 13 June 2022.

Kuvarega, A.T., Khumalo, N., Dlamini, D., Mamba, B.B., 2018. Polysulfone/N,Pd co-doped TiO₂ composite membranes for photocatalytic dye degradation. *Separation and Purification Technology*. Vol. 191, pp. 122. DOI 10.1016/J.SEPPUR.2017.07.064.

Lavorato, C., Argurio, P., Mastropietro, T.F., Pirri, G., Poerio, T., Molinari, R., 2017. Pd/TiO₂ doped faujasite photocatalysts for acetophenone transfer hydrogenation in a photocatalytic membrane reactor. *Journal of Catalysis*. Vol. 353, pp. 152. DOI 10.1016/J.JCAT.2017.07.015.

Leong, S., Razmjou, A., Wang, K., Hapgood, K., Zhang, X., Wang, H., 2014. TiO₂ based photocatalytic membranes: A review. *Journal of Membrane Science*. Vol. 472, pp. 167. DOI 10.1016/J.MEMSCI.2014.08.016.

Li, H., Yang, Y., Gao, J., Li, X., Zhou, Z., Wang, N., Du, P., Zhang, T., Feng, J., 2020. Degradation of sodium dodecyl benzenesulfonate by vacuum ultraviolet irradiation. *Journal of Water Process Engineering*. Vol. 34, pp. 101172. DOI 10.1016/j.jwpe.2020.101172.

Liu, B., Yu, Z., Song, X., Yang, F., 2010. Effects of sodium dodecylbenzene sulfonate and sodium dodecyl sulfate on the *Mytilus galloprovincialis* biomarker system. *Ecotoxicology and Environmental Safety*. Vol. 73, no. 5, pp. 835. DOI 10.1016/j.ecoenv.2009.12.011.

Liu, L., Luo, X.B., Ding, L., Luo, S.L., 2019. Application of Nanotechnology in the Removal of Heavy Metal From Water. In: *Nanomaterials for the Removal of Pollutants and Resource Reutilization*. Elsevier. pp. 83.

Ma, N., Zhang, Y., Quan, X., Fan, X., Zhao, H., 2010. Performing a microfiltration integrated with photocatalysis using an Ag-TiO₂/HAP/Al₂O₃ composite membrane for water treatment: Evaluating effectiveness for humic acid removal and anti-fouling properties. *Water Research*. Vol. 44, no. 20, pp. 6104. DOI 10.1016/J.WATRES.2010.06.068.

Madjene, F., Aoudjit, L., Igoud, S., Lebig, H., Boutra, B., 2013. A review: titanium dioxide photocatalysis for water treatment. *Transition Journal of Science and Technology*. Vol. 3, no. 10. ISSN 1857-8047.

Manousaki, E., Psillakis, E., Kalogerakis, N., Mantzavinos, D., 2004. Degradation of sodium dodecylbenzene sulfonate in water by ultrasonic irradiation. *Water Research*. Vol. 38, no. 17, pp. 3751. DOI 10.1016/j.watres.2004.06.002.

Mantecón-Oria, M., Diban, N., Berciano, M.T., Rivero, M.J., David, O., Lafarga, M., Tapia, O., Urtiaga, A., 2020. Hollow Fiber Membranes of PCL and PCL/Graphene as Scaffolds with

Potential to Develop In Vitro Blood—Brain Barrier Models. *Membranes*. Vol. 10, no. 8, pp. 161. DOI 10.3390/MEMBRANES10080161.

Masoudian, Z., Salehi-Lisar, S.Y., Norastehnia, A., 2020. Phytoremediation potential of *Azolla filiculoides* for sodium dodecyl benzene sulfonate (SDBS) surfactant considering some physiological responses, effects of operational parameters and biodegradation of surfactant. *Environmental Science and Pollution Research*. Vol. 27, no. 16, pp. 20358. DOI 10.1007/s11356-020-08286-2.

Moulai-Mostefa, N., Ding, L.H., Frappart, M., Jaffrin, M.Y., 2007. Treatment of Aqueous Ionic Surfactant Solutions by Dynamic Ultrafiltration. *Separation Science and Technology*. Vol. 42, no. 12, pp. 2583. DOI 10.1080/01496390701526612.

Moura, L., Picão, R.C., 2022. Removal of antimicrobial resistance determinants from wastewater: a risk perspective on conventional and emerging technologies. *Emerging Contaminants in the Environment*. pp. 603. DOI 10.1016/B978-0-323-85160-2.00023-8.

Mungray, A.K., Kumar, P., 2009. Fate of linear alkylbenzene sulfonates in the environment: A review. *International Biodeterioration & Biodegradation*. Vol. 63, no. 8, pp. 981. DOI 10.1016/j.ibiod.2009.03.012.

Nakama, Y., 2017. Surfactants. In: *Cosmetic Science and Technology*. Elsevier. pp. 231.

Nakata, K., Fujishima, A., 2012. TiO₂ photocatalysis: Design and applications. *Journal of Photochemistry and Photobiology C: Photochemistry Reviews*. Vol. 13, no. 3, pp. 169. DOI 10.1016/J.JPHOTOCHEMREV.2012.06.001.

Nielsen, A.M., Britton, L.N., Beall, C.E., McCormick, T.P., Russell, G.L., 1997. Biodegradation of coproducts of commercial linear alkylbenzene sulfonate. *Environmental Science and Technology*. Vol. 31, no. 12, pp. 3397. DOI 10.1021/ES970023M.

Ochiai, T., Fujishima, A., 2012. Photoelectrochemical properties of TiO₂ photocatalyst and its applications for environmental purification. *Journal of Photochemistry and Photobiology C: Photochemistry Reviews*. Vol. 13, no. 4, pp. 247. DOI 10.1016/J.JPHOTOCHEMREV.2012.07.001.

Palmer, M., Hatley, H., 2018. The role of surfactants in wastewater treatment: Impact, removal and future techniques: A critical review. *Water Research*. Vol. 147, pp. 60. DOI 10.1016/j.watres.2018.09.039.

Pastrana-Martínez, L.M., Morales-Torres, S., Pérez-Molina, Á., Maldonado-Hódar, F.J., 2021. Photocatalytic membranes: Synthesis, properties, and applications. *Photocatalytic Systems by Design: Materials, Mechanisms and Applications*. pp. 385. DOI 10.1016/B978-0-12-820532-7.00018-7.

Pendergast, M.M., Hoek, E.M.V., 2011. A review of water treatment membrane nanotechnologies. *Energy & Environmental Science*. Vol. 4, no. 6, pp. 1946. [Accessed 28 June 2022]. DOI 10.1039/C0EE00541J.

Peyravi, M., Jahanshahi, M., Mona Mirmousaei, S., Lau, W.J., 2021. Dynamically Coated Photocatalytic Zeolite–TiO₂ Membrane for Oil-in-Water Emulsion Separation. *Arabian Journal*

for Science and Engineering. Vol. 46, no. 7, pp. 6143. DOI 10.1007/S13369-019-04335-2/TABLES/4.

Pinnau, I., 2000. MEMBRANE SEPARATIONS | Membrane Preparation. In: *Encyclopedia of Separation Science*. Elsevier. pp. 1755.

PWC, 2018. La gestión del agua en España. Análisis y retos del ciclo urbano del agua. <https://www.pwc.es/es/publicaciones/energia/assets/gestion-agua-2018-espana.pdf>. 18 May 2022.

Registration Dossier - ECHA, 2022. <https://echa.europa.eu/es/registration-dossier/-/registered-dossier/11639/4/1> 29 June 2022.

Reinoso, D., Adrover, M., Pedernera, M., 2018. Green synthesis of nanocrystalline faujasite zeolite. *Ultrasonics Sonochemistry*. 2018. Vol. 42, pp. 303. DOI 10.1016/j.ultsonch.2017.11.034.

Riaz, S., Park, S.J., 2020. An overview of TiO₂-based photocatalytic membrane reactors for water and wastewater treatments. *Journal of Industrial and Engineering Chemistry*. Vol. 84, pp. 23. DOI 10.1016/J.JIEC.2019.12.021.

Ribao, P., Corredor, J., Rivero, M.J. And Ortiz, I., 2019. Role of reactive oxygen species on the activity of noble metal-doped TiO₂ photocatalysts. *Journal of Hazardous Materials*. Vol. 372, pp. 45. DOI 10.1016/J.JHAZMAT.2018.05.026.

Ribao, P., Rivero, M.J. And Ortiz, I., 2017. TiO₂ structures doped with noble metals and/or graphene oxide to improve the photocatalytic degradation of dichloroacetic acid. *Environmental Science and Pollution Research*. Vol. 24, no. 14, pp. 12628. DOI 10.1007/S11356-016-7714-X/FIGURES/9.

Ribao, P., Rivero, M.J. And Ortiz, I., 2018. Enhanced photocatalytic activity using GO/TiO₂ catalyst for the removal of DCA solutions. *Environmental Science and Pollution Research*. Vol. 25, no. 35, pp. 34893. DOI 10.1007/S11356-017-0901-6/FIGURES/7.

Ritchie, H., Roser, M., 2017. Water Use and Stress. <https://ourworldindata.org/water-use-stress>. 22 April 2022.

Rivero, M.J., Ribao, P., Gomez-Ruiz, B., Urriaga, A., Ortiz, I., 2020. Comparative performance of TiO₂-rGO photocatalyst in the degradation of dichloroacetic and perfluorooctanoic acids. *Separation and Purification Technology*. Vol. 240, pp. 116637. DOI 10.1016/J.SEPPUR.2020.116637.

Romay, M., Diban, N., Rivero, M.J., Urriaga, A., Ortiz, I., 2020. Critical Issues and Guidelines to Improve the Performance of Photocatalytic Polymeric Membranes. *Catalysts*. Vol. 10, no. 5, pp. 570. DOI 10.3390/CATAL10050570.

Sanchez, M., Rivero, M.J., Ortiz, I., 2011. Kinetics of dodecylbenzenesulphonate mineralisation by TiO₂ photocatalysis. *Applied Catalysis B: Environmental*. Vol. 101, no. 3, pp. 515. DOI 10.1016/J.APCATB.2010.10.023.

Sánchez-González, S., Diban, N., Bianchi, F., Ye, H., Urriaga, A., 2018. Evidences of the Effect of GO and rGO in PCL Membranes on the Differentiation and Maturation of Human Neural

Progenitor Cells. *Macromolecular Bioscience*. Vol. 18, no. 11, pp. 1800195. DOI 10.1002/MABI.201800195.

Sánchez-González, S., Diban, N., Urriaga, A., 2018. Hydrolytic Degradation and Mechanical Stability of Poly(ϵ -Caprolactone)/Reduced Graphene Oxide Membranes as Scaffolds for In Vitro Neural Tissue Regeneration. *Membranes*. Vol. 8, no. 1, pp. 12. DOI 10.3390/MEMBRANES8010012.

Satheesh Ananda, S., Mehendale, H.M., 2005. Chlorination By-Products. *Encyclopedia of Toxicology*. pp. 546. DOI 10.1016/B0-12-369400-0/00214-3.

Seery, M.K, George, R., Floris, P., Pillai, S.C, 2007. Silver doped titanium dioxide nanomaterials for enhanced visible light photocatalysis. *Journal of Photochemistry and Photobiology A: Chemistry*. Vol. 189, no. 2, pp. 258. DOI 10.1016/j.jphotochem.2007.02.010.

Shareef, U., Waqas, M., 2020. Bisphenol A Removal through Low-Cost Kaolin-Based Ag@TiO₂ Photocatalytic Hollow Fiber Membrane from the Liquid Media under Visible Light Irradiation. *Journal of Nanomaterials*. Vol. 2020. DOI 10.1155/2020/3541797.

Shi, Y., Yang, D., Li, Y., Qu, J., Yu, Z.Z, 2017. Fabrication of PAN@TiO₂/Ag nanofibrous membrane with high visible light response and satisfactory recyclability for dye photocatalytic degradation. *Applied Surface Science*. Vol. 426, pp. 622. DOI 10.1016/j.apsusc.2017.06.302.

Song, Z., Fathizadeh, M., Huang, Y., Chu, K.H, Yoon, Y., Wang, L., Xu, W.L., Yu, M., 2016. TiO₂ nanofiltration membranes prepared by molecular layer deposition for water purification. *Journal of Membrane Science*. Vol. 510, pp. 72. DOI 10.1016/J.MEMSCI.2016.03.011.

Substance Information - ECHA, 2022. <https://echa.europa.eu/es/substance-information/-/substanceinfo/100.001.098> 29 June 2022.

Sumpter, S.R., 2000. ENVIRONMENTAL APPLICATIONS | Pressurized Fluid Extraction. In: *Encyclopedia of Separation Science*. Elsevier. pp. 2687.

Synthetic zeolites - structure, classification, current trends in zeolite synthesis review, 2022. https://www.researchgate.net/publication/322211658_SYNTHETIC_ZEOLITES_-_STRUCTURE_CLASIFICACION_CURRENT_TRENDS_IN_ZEOLITE_SYNTHESIS_REVIEW 11 June 2022.

Taffarel, S.R., Rubio, J., 2010. Adsorption of sodium dodecyl benzene sulfonate from aqueous solution using a modified natural zeolite with CTAB. *Minerals Engineering*. Vol. 23, no. 10, pp. 771. DOI 10.1016/j.mineng.2010.05.018.

Tang, Y., Yin, M., Yang, W., Li, H., Zhong, Y., Mo, L., Liang, Y., Ma, X., Sun, X., 2019. Emerging pollutants in water environment: Occurrence, monitoring, fate, and risk assessment. *Water Environment Research*. Vol. 91, no. 10, pp. 984. DOI 10.1002/wer.1163.

Tiseo, I., 2022. Distribution of water withdrawals worldwide as of 2018, by sector. <https://www.statista.com/statistics/1258433/water-withdrawals-shares-worldwide-by-sector/>. 29 June 2022.

Tu, Z., Ding, L., Frappart, M., Jaffrin, M.Y, 2009. Studies on treatment of sodium dodecyl benzene sulfonate solution by high shear ultrafiltration system. *Desalination*. Vol. 240, no. 1, pp. 251. DOI 10.1016/j.desal.2008.01.051.

UNEP - UN ENVIRONMENT PROGRAMME, 2022. Emerging Pollutants in Wastewater: An Increasing Threat. <http://www.unep.org/events/un-environment-event/emerging-pollutants-wastewater-increasing-threat>. 3 May 2022.

UNICEF, 2019. 1 in 3 people globally do not have access to safe drinking water. <https://www.who.int/news/item/18-06-2019-1-in-3-people-globally-do-not-have-access-to-safe-drinking-water-unicef>. 3 May 2022.

Venhuis, S.H., Mehrvar, M., 2004. Health effects, environmental impacts, and photochemical degradation of selected surfactants in water. *International Journal of Photoenergy*. Vol. 6, no. 3, pp. 115. DOI 10.1155/S1110662X04000157.

Vinoth Kumar, R., Ganesh Moorthy, I., Pugazhenth, G., 2017. Separation of BSA through FAU-type zeolite ceramic composite membrane formed on tubular ceramic support: Optimization of process parameters by hybrid response surface methodology and biobjective genetic algorithm. Vol. 47, no. 7, pp. 687. DOI 10.1080/10826068.2017.1303608.

Vital-Grappin, A.D., Ariza-Tarazona, M.C., Luna-Hernández, V.M., Villarreal-Chiu, J.F., Hernández-López, J.M., Siligardi, C., Cedillo-González, E.I., 2021. The role of the reactive species involved in the photocatalytic degradation of HDPE microplastics using C, N-TiO₂ powders. *Polymers*. Vol. 13, no 7, p. 999. DOI 10.3390/polym13070999.

WHO, 2005. Dichloroacetic Acid in Drinking-water Background document for development of WHO Guidelines for Drinking-water Quality. https://cdn.who.int/media/docs/default-source/wash-documents/wash-chemicals/dichloroaceticacid0505.pdf?sfvrsn=2246389b_4 13 March 2022.

Workneh, S., Shukla, A., 2008. Synthesis of sodalite octahydrate zeolite-clay composite membrane and its use in separation of SDS. *Journal of Membrane Science*. 2008. Vol. 309, no. 1, pp. 189. DOI 10.1016/j.memsci.2007.10.033.

Xiang, Q., Fukahori, S., Yamashita, N., Tanaka, H., Fujiwara, T., 2017. Removal of Crotamiton from Reverse Osmosis Concentrate by a TiO₂/Zeolite Composite Sheet. *Applied Sciences*. Vol. 7, no. 8, pp. 778. DOI 10.3390/APP7080778.

Yu, X., Trapp, S., Zhou, P., Peng, X., Cao, X., 2006. Response of weeping willows to linear alkylbenzene sulfonate. *Chemosphere*. Vol. 64, no. 1, pp. 43. DOI 10.1016/j.chemosphere.2005.11.025.

Zhang, F., Wang, X., Liu, H., Liu, C., Wan, Y., Long, Y., Cai, Z., 2019. Recent Advances and Applications of Semiconductor Photocatalytic Technology. *Applied Sciences*. Vol. 9, no. 12, pp. 2489. DOI 10.3390/APP9122489.

Zhang, H., Quan, X., Chen, S., Zhao, H., Zhao, Y., 2006. The removal of sodium dodecylbenzene sulfonate surfactant from water using silica/titania nanorods/nanotubes composite membrane with photocatalytic capability. *Applied Surface Science*. Vol. 252, no. 24, pp. 8598. DOI 10.1016/J.APSUSC.2005.11.090.

Zhang, Z., Deng, Y., Shen, M., Han, W., Chen, Z., Xu, D., Ji, X., 2009. Investigation on rapid degradation of sodium dodecyl benzene sulfonate (SDBS) under microwave irradiation in the presence of modified activated carbon powder with ferrous sulfate. *Desalination*. Vol. 249, no. 3, pp. 1022. DOI 10.1016/j.desal.2009.09.010.

Zhu, F.J., Ma, W.L., Xu, T.F., Ding, Y., Zhao, X., Li, W.L., Liu, L.Y., Song, W.W., Li, Y.F., Zhang, Z.F., 2018. Removal characteristic of surfactants in typical industrial and domestic wastewater treatment plants in Northeast China. *Ecotoxicology and Environmental Safety*. Vol. 153, pp. 84. DOI 10.1016/j.ecoenv.2018.02.001.

8. APPENDIX

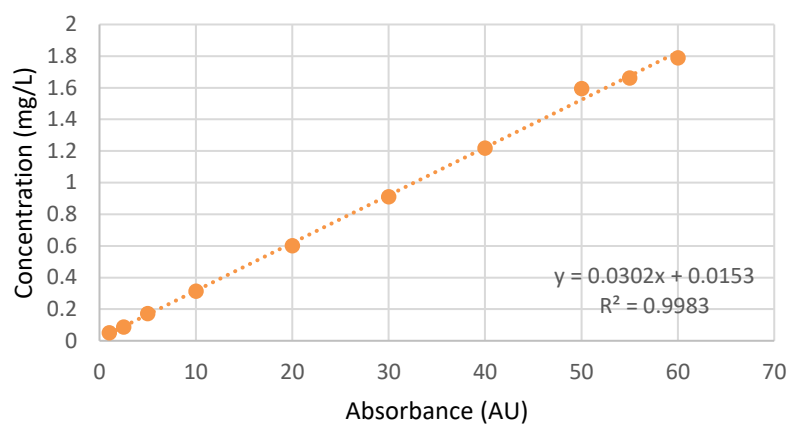


Figure 1A. DBS calibration curve